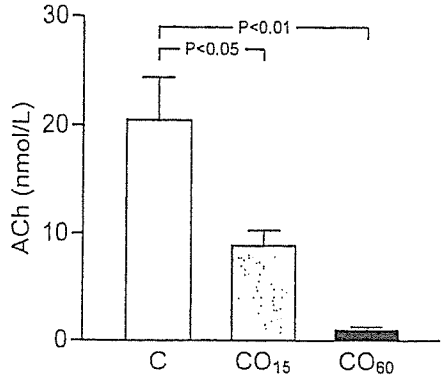

Fig. 2. Myocardial interstitial ACh response to electrical vagal stimulation obtained from *protocol 1*. The ACh response was attenuated in the CO_{15} group and abolished in the CO_{60} group compared with the C (control) group.

thereby locally administering ouabain through the dialysis probe. Local ouabain administration was performed in control animals (n = 8), animals with vagotomy (VX group, n = 6), and animals with intact vagi subjected to 60-min ischemia followed by 60-min reperfusion (CO group, n = 6).

Statistical analysis. All data are presented as means ± SE. In *protocol 1*, differences in the electrical stimulation-induced ACh release among control, CO_{15}, and CO_{60} groups were examined by using one-way ANOVA followed by Dunnett's test (7). In *protocol 2*, changes in the ACh concentration in the CO group were examined by using a repeated-measures ANOVA. When there was significant difference, Dunnett's test was applied to identify the difference relative to the baseline ACh concentration. We also examined differences in the baseline or maximum ACh responses among the control, VX, and CO groups by using one-way ANOVA, followed by Dunnett's test. Differences were considered significant when $P < 0.05$.

RESULTS

Figure 2 shows ACh liberated into the myocardial interstitium in response to vagal stimulation in *protocol 1*. The electrical stimulation-induced ACh response was suppressed in the CO_{15} group compared with the control group and abolished in the CO_{60} group.

Figure 3 depicts changes in the myocardial interstitial ACh level in response to local ouabain administration in the CO group obtained from *protocol 2*. The ACh level increased gradually on ouabain administration, reaching a maximum at 15–30 min, after which it declined toward baseline.

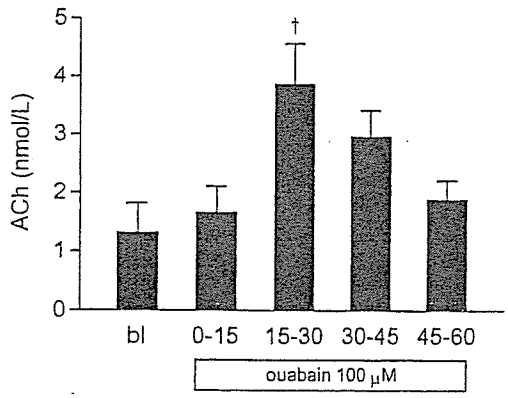

Fig. 3. Myocardial interstitial ACh response to local ouabain administration through the dialysis probe obtained in the CO group in *protocol 2*. The ACh level was increased significantly from the baseline value after 15–30 min of ouabain administration. †$P < 0.05$.

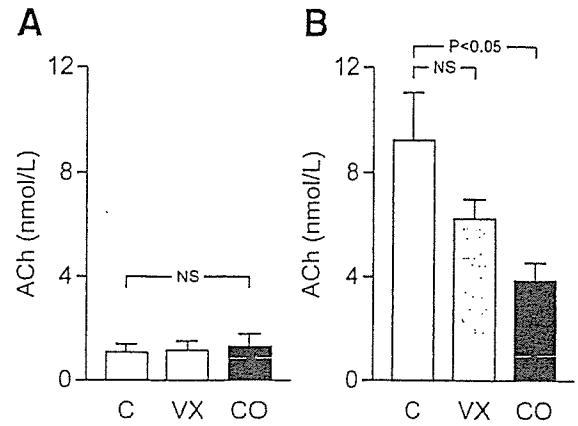

Fig. 4. Effects of local ouabain administration on the myocardial interstitial ACh levels obtained from *protocol 2*. *A*: baseline ACh levels for control, VX, and CO groups. *B*: maximum ACh levels obtained after 15–30 min of ouabain administration for control, VX, and CO groups.

Figure 4*A* illustrates the baseline ACh levels in *protocol 2*. There were no significant differences in baseline ACh levels among control, VX, and CO groups. Figure 4*B* illustrates the maximum ACh responses observed during 15–30 min of ouabain administration. The CO group exhibited a significantly reduced ACh response compared with the control group. The VX group showed the maximum ACh response between the control and CO groups.

Table 1 summarizes mean arterial pressure (MAP) and HR obtained from the CO group in *protocol 2*. Changes in MAP and HR 60 min after LAD occlusion and 60 min after reperfusion were insignificant compared with preocclusion values.

DISCUSSION

To our knowledge, this is the first report on in vivo ACh release in the postischemic myocardium. The finding is in marked contrast to observations of ischemia-induced ACh release in our previous studies (10–13). The following discussion will focus on two aspects: postischemic deterioration of axonal conduction and nerve terminal function of the vagal efferent nerve.

Interruption of vagal efferent neuronal function. Myocardial interstitial ACh release in response to electrical stimulation of the vagi was suppressed markedly

Table 1 *Changes in MAP and HR in animals with intact vagi*

	Pre	CO	Rep
MAP, mmHg	112 ± 7	105 ± 8	100 ± 7
HR, beats/min	192 ± 11	168 ± 6	172 ± 9

Values are means ± SE. Data were obtained at preocclusion (Pre), 60-min after occlusion (CO), and 60-min after reperfusion (Rep) of the left anterior descending coronary artery. MAP, mean arterial pressure; HR, heart rate.

60 min after reperfusion after LAD occlusion in the presence of occlusions lasting 15 or 60 min (Fig. 2). The attenuation of the ACh response to electrical stimulation in the CO_{60} group was similar to that achieved by pretreatment with a voltage-sensitive Na^+ channel inhibitor, tetrodotoxin (13), suggesting complete damage to vagal efferent neuronal function in the postischemic myocardium. Because ouabain-induced ACh release was not abolished in the CO group in *protocol 2* (Fig. 3), the disruption of vagal efferent neuronal function can be attributed mainly to damage to vagal axons. Inoue and Zipes (8) demonstrated that the vagal efferent neuronal function, assessed by the lengthening of the effective refractory period in the nonischemic myocardium apical to the ischemic region, is impaired heterogenously 5–20 min after coronary artery occlusion. The present results indicate that the disruption of the vagal efferent axons in the postischemic myocardium persists for at least 60 min after LAD reperfusion began.

It is unlikely that the LAD occlusion exerted mechanical damage to the intracardiac vagal efferent axons. The reasons are as follows. First, most vagal efferent fibers cross the atrioventricular groove dive intramurally and are located in the subendocardium in the ventricle (22). Therefore, the vagal efferent fibers run apart from the LAD ligation snare. Second, the suppression of electrical stimulation-induced ACh release depended on the duration of LAD occlusion (Fig. 2). If the vagal efferent fibers were mechanically damaged by the ligation procedure, an abrupt interruption of electrical stimulation-induced ACh release should have resulted. The fact that 5-min brief LAD occlusion followed by 20-min reperfusion did not suppress the ACh release in response to subsequent 5-min brief LAD occlusion in a previous study (11) is also in opposition to the possible mechanical damage to the intracardiac vagal efferent axons by the ligation procedure.

Impaired local ACh release. Our previous studies indicated that acute myocardial ischemia increases myocardial interstitial ACh levels in the ischemic region (10, 12). In those studies, vagotomy did not abolish ischemia-induced ACh release, suggesting that a local release mechanism independent of the centrally mediated vagal control plays a significant role in the ischemia-induced ACh release. Whereas no significant differences were observed in MAP and HR 60 min after ischemia and reperfusion compared with preischemic baseline values (Table 1), marked ACh release evoked by acute myocardial ischemia might have caused depletion of ACh stores or structural membrane abnormalities in the vagal efferent nerve terminals. Although the baseline ACh levels were similar between the control and CO groups (Fig. 4), this does not guarantee functional recovery of the vagal nerve terminals in the postischemic myocardium. To assess the functional recovery of the vagal nerve terminals more precisely, we examined the effect of local ouabain administration on the myocardial interstitial ACh levels.

Integrity of the axoplasmic membrane may be judged by normal Na^+-K^+-ATPase activity. Ouabain inhibits the membrane Na^+-K^+-ATPase and induces intracellular Na^+ accumulation, which leads to exocytotic ACh release via the reversal of Na^+/Ca^{2+} exchanger, activation of voltage-sensitive Ca^{2+} channels, and/or intracellular Ca^{2+} mobilization (16, 18). Because Na^+-K^+-ATPase is the major target for ATP at the nerve terminal, ischemia induces a progressive failure of Na^+-K^+-ATPase activity by depletion of ATP. If the integrity of the axoplasmic membrane had been lost due to ischemia and the Na^+-K^+-ATPase remained inactive after reperfusion, ouabain would not be able to evoke ACh release in the postischemic myocardium. Similarly, if the ACh stores were depleted by ischemia-induced ACh release, ouabain would also fail to induce ACh release. However, ouabain increased ACh levels in CO group (Fig. 3), indicating that membrane function was restored within 60 min after reperfusion. The observed result is consistent with the fact that the Na^+-K^+-ATPase becomes active on reperfusion, leading to restoration of the Na^+ gradient across the axoplasmic membrane in isolated rat hearts (19).

Whereas ouabain administration evoked myocardial interstitial ACh release, the ACh levels so induced were lower in the CO than in the control group (Fig. 4). To examine whether the difference in ouabain-induced ACh release is associated with the absence of baseline vagal activity, we performed local ouabain administration in vagotomized animals. As shown in Fig. 4*B*, the VX group showed that ACh levels were in between the control and CO groups. Therefore, absence of the baseline vagal activity due to the interruption of axonal conduction, on top of the impaired local ACh release, could contribute to the suppression of ouabain-induced ACh release in the CO group. According to a study by Schmid et al. (17), changes in the activity of choline acetyltransferase in ischemic myocardial tissue are insignificant 2.5 and 5 h after coronary artery occlusion. The discrepancy between ACh synthesis and ouabain-induced ACh release suggests that nerve terminal function depends not only on axoplasmic enzyme activity but also on extraneuronal circumstances, such as extracellular ion content.

Limitations. Methodological limitations associated with anesthesia and eserine administration have been described previously (10–13). Other limitations to the present study are as follows. First, we did not examine whether vagal efferent function after LAD occlusion was reversible in the long term. To answer this question, further studies focusing on the recovery of vagal efferent function by using chronic experimental models are required. Second, we did not assess the impact of disruption of the vagal efferent neuronal function on the arrhythmogenesis. Vagal nerve activity is known to exert both antiarrhythmic and proarrhythmic effects on the heart (6). Further studies are clearly needed to elucidate the functional significance of the disruption of the vagal control on the postischemic cardiac events.

In conclusion, we found interruption of the myocardial ACh release in response to vagal stimulation as well as suppression of local ACh release in the postischemic myocardium 60 min after reperfusion after

60-min LAD occlusion. The disruption of vagal control in the postischemic myocardium might have deleterious effects on the heart.

This study was supported by Ministry of Health and Welfare of Japan, Cardiovascular Diseases Research Grants 9C-1, 11C-3, 11C-7; a Health Sciences Research Grant for Advanced Medical Technology; a National Space Development Agency of Japan and Japan Space Forum Grant; a Ground-Based Research Grant for the Space Utilization; a Science and Technology Agency of Japan Grant; a Bilateral International Joint Research Grant; Ministry of Education, Science, Sports and Culture of Japan Grants; Scientific Research Grants-in-Aid B-11694337, C-11680862, C-11670730; Encouragement of Young Scientists Grants-in-Aid 11770390 and 11770391; and by a Japan Science and Technology Corporation, Research and Development Grant for Applying Advanced Computational Science and Technology.

REFERENCES

1. **Akiyama T and Yamazaki T.** Norepinephrine release from cardiac sympathetic nerve endings in the in vivo ischemic region. *J Cardiovasc Pharmacol* 34: S11–S14, 1999.
2. **Akiyama T, Yamazaki T, and Ninomiya I.** In vivo detection of endogenous acetylcholine release in cat ventricles. *Am J Physiol Heart Circ Physiol* 266: H854–H860, 1994.
3. **Armour JA.** Myocardial ischemia and the cardiac nervous system. *Cardiovasc Res* 41: 41–54, 1999.
4. **Barber MJ, Mueller TM, Henry DP, Felten SY, and Zipes DP.** Transmural myocardial infarction in the dog produces sympathectomy in noninfarcted myocardium. *Circulation* 67: 787–796, 1983.
5. **Ciuffo AA, Ouyang P, Becker LC, Levin L, and Weisfeldt ML.** Reduction of sympathetic inotropic response after ischemia in dogs. *J Clin Invest* 75: 1504–1509, 1985.
6. **Corr PB and Gillis RA.** Autonomic neural influences on the dysrhythmias resulting from myocardial infarction. *Circ Res* 43: 1–9, 1978.
7. **Glantz SA.** *Primer of Biostatistics* (5th ed.). New York: McGraw-Hill, 2002.
8. **Inoue H and Zipes DP.** Time course of denervation of efferent sympathetic and vagal nerves after occlusion of the coronary artery in the canine heart. *Circ Res* 62: 1111–1120, 1988.
9. **Janes RD, Johnstone DE, and Armour JA.** Functional integrity of intrinsic cardiac nerves located over an acute transmural myocardial infarction. *Can J Physiol Pharmacol* 65: 64–69, 1986.
10. **Kawada T, Yamazaki T, Akiyama T, Inagaki M, Shishido T, Zheng C, Yanagiya Y, Sugimachi M, and Sunagawa K.** Vagosympathetic interactions in ischemia-induced myocardial norepinephrine and acetylcholine release. *Am J Physiol Heart Circ Physiol* 280: H216–H221, 2001.
11. **Kawada T, Yamazaki T, Akiyama T, Mori H, Inagaki M, Shishido T, Takaki H, Sugimachi M, and Sunagawa K.** Effects of brief ischaemia on myocardial acetylcholine and noradrenaline levels in anaesthetized cats. *Auton Neurosci* 95: 37–42, 2002.
12. **Kawada T, Yamazaki T, Akiyama T, Sato T, Shishido T, Inagaki M, Takaki H, Sugimachi M, and Sunagawa K.** Differential acetylcholine release mechanisms in the ischemic and non-ischemic myocardium. *J Mol Cell Cardiol* 32: 405–414, 2000.
13. **Kawada T, Yamazaki T, Akiyama T, Shishido T, Inagaki M, Uemura K, Miyamoto T, Sugimachi M, Takaki H, and Sunagawa K.** In vivo assessment of acetylcholine-releasing function at cardiac vagal nerve terminals. *Am J Physiol Heart Circ Physiol* 281: H139–H145, 2001.
14. **Lameris TW, de Zeeuw S, Alberts G, Boomsma F, Duncker DJ, Verdouw PD, Veld AJ, and van den Meiracker AH.** Time course and mechanism of myocardial catecholamine release during transient ischemia in vivo: *Circulation* 101: 2645–2650, 2000.
15. **Miyazaki T and Zipes DP.** Presynaptic modulation of efferent sympathetic and vagal neurotransmission in the canine heart by hypoxia, high K^+, low pH, and adenosine. *Circ Res* 66: 289–301, 1990.
16. **Satoh E and Nakazato Y.** On the mechanism of ouabain-induced release of acetylcholine from synaptosomes. *J Neurochem* 58: 1038–1044, 1992.
17. **Schmid PG, Greif BJ, Lund DD, and Roskoski R Jr.** Tyrosine hydroxylase and choline acetyltransferase activities in ischemic canine heart. *Am J Physiol Heart Circ Physiol* 243: H788–H795, 1982.
18. **Török TL.** Neurochemical transmission and the sodium-pump. *Prog Neurobiol* 32: 11–76, 1989.
19. **Van Emous JG, Schreur JHM, Ruigrok TJC, and van Echteld CJA.** Both Na^+-K^+ ATPase and Na^+-H^+ exchanger are immediately active upon post-ischemic reperfusion in isolated rat heart. *J Mol Cell Cardiol* 30: 337–348, 1998.
20. **Yamazaki T, Akiyama T, and Kawada T.** Effects of ouabain on in situ cardiac sympathetic nerve endings. *Neurochem Int* 35: 439–445, 1999.
21. **Yamazaki T, Akiyama T, Kawada T, Kitagawa H, Takauchi Y, Yahagi N, and Sunagawa K.** Norepinephrine efflux evoked by potassium chloride in cat sympathetic nerves: dual mechanism of action. *Brain Res* 794: 146–150, 1998.
22. **Zipes DP.** Influence of myocardial ischemia and infarction on autonomic innervation of heart. *Circulation* 82: 1095–1105, 1990.

ELSEVIER

Neuroscience Letters 324 (2002) 232–236

Neuroscience Letters

www.elsevier.com/locate/neulet

Modulatory effects of ketamine on catecholamine efflux from in vivo cardiac sympathetic nerve endings in cats

Hirotoshi Kitagawa[a], Toji Yamazaki[b,*], Tsuyoshi Akiyama[b], Naoki Yahagi[b], Toru Kawada[c], Hidezo Mori[b], Kenji Sunagawa[c]

[a]*Department of Anesthesia, Nagahama City Hospital, Nagahama, Japan*
[b]*Department of Cardiac Physiology, National Cardiovascular Center, Research Institute, Suita, Osaka 565-8565, Japan*
[c]*Department of Cardiovascular Dynamics National Cardiovascular Center, Research Institute, Suita, Osaka, Japan*

Received 28 December 2001; received in revised form 18 February 2002; accepted 20 February 2002

Abstract

With the use of the microdialysis technique, we examined the modulatory effect of ketamine on catecholamine efflux from in vivo cardiac sympathetic nerve endings. A dialysis probe was implanted in the left ventricular myocardium, and dialysate norepinephrine (NE) levels in anesthetized cats were measured with liquid chromatogram–electrical detection. A 60-min occlusion of the left anterior descending coronary artery caused increases in dialysate NE levels. Through the dialysis probe, locally applied ketamine (10 mM) augmented the dialysate NE responses to coronary occlusion in the presence and absence of desipramine (membrane NE transport blocker). Thus, the ketamine-induced NE increment is not mediated through the neuronal NE transporter. The sympathomimetic action of ketamine may augment the NE efflux evoked by myocardial ischemia. © 2002 Published by Elsevier Science Ireland Ltd.

Keywords: Epinephrine; Norepinephrine; Dialysis technique; Ischemia; Heart; Transporter

Ketamine has been widely used as an anesthetic. In addition to its anesthetic action, ketamine has been reported to provide neuronal protection from ischemic [14] and hypoxic injury [13,22]. Ketamine, at the relatively high concentration of 1 mM, tends to protect hippocampal neurons in culture from anoxia [15] and protects against neuronal ischemic injury in the gerbil [11]. In these pathological conditions, ketamine seems to suppress the neurotransmitter release evoked by anoxia or ischemia. Up to now, several actions and mechanisms for this neuronal protection have been proposed from in vitro studies: *N*-methyl-D-aspartate antagonist [27]; Na^+ channel blockers [28]; and/or inhibitory action on neurotransmitter transporter [2,17]. In ischemia or anoxia, the glutamate transporter runs in the reverse direction due to the reduced Na^+ gradient and releases glutamate from the axoplasmic site to the extracellular space [2,12]. Taking into consideration this releasing mechanism, the effect of ketamine might be related to its inhibitory action on the neurotransmitter transporter.

In the sympathetic nerve endings, ischemia or hypoxia evokes an efflux of norepinephrine (NE) through the outward movement of the NE transporter similar to the glutamate transporter [5,18]. More recently, several studies have demonstrated that ketamine inhibits the monoamine transporter expressed in cultured cells [6,20]. These data indicate the possibility that ketamine suppresses the NE release evoked by myocardial ischemia. On the other hand, ketamine has been reported to exert a sympathomimetic action [4,16], which may exacerbate the NE efflux evoked by ischemia. It is uncertain whether ketamine induces suppression or augmentation of the NE efflux induced by myocardial ischemia.

In the present study, we applied a dialysis technique to the heart of anesthetized cats [1] and investigated the dialysate NE response during local administration of ketamine through the dialysis probe. Further, we examined whether ketamine modulates the release of NE and epinephrine (Epi) evoked by coronary occlusion.

Animal care proceeded in strict accordance with the guiding principles of the Physiological Society of Japan. Twenty-eight adult cats of either sex (2.2–4.5 kg) were anesthetized with pentobarbital (30–35 mg/kg i.p.). The level of anesthesia was maintained by a continuous infusion of pentobarbital (1–2 mg/kg per h). The animals were

* Corresponding author. Tel.: +81-6-6833-5012; fax: +81-6-6872-8092.
E-mail address: yamazaki@ri.ncvc.go.jp (T. Yamazaki).

0304-3940/02/$ - see front matter © 2002 Published by Elsevier Science Ireland Ltd.
PII: S0304-3940(02)00208-2

immobilized with pancuronium (0.5 mg/h i.v.) and ventilated with room air mixed with oxygen. Body temperature was maintained with a heating pad and lamp. Arterial pressure and heart rate were simultaneously monitored. After left side thoracotomy, a dialysis probe was implanted in the left anterior descending coronary artery (LAD) perfused region of the left ventricle wall along the long axis. A 4-0 silk suture was passed around the LAD just distal to the first diagonal branch, taking care to prevent damage to the pericoronary nerve, and the ends of the suture were threaded through a small vinyl tube to make a snare for later coronary occlusion. Heparin sodium (100 units/kg) was intravenously administered to prevent blood coagulation.

We measured dialysate NE and Epi levels as indices of myocardial interstitial NE and EP levels, respectively [1]. The material and properties are described elsewhere [1]. Briefly, a dialysis fiber (13 mm × 0.2 mm I.D.; PAN-1200, 50,000 molecular weight cut-off; Asahi Chemical, Tokyo, Japan) was glued at both ends to a polyethylene tube. The dialysis probes were perfused with Ringer Solution at a rate of 2–10 μl/min. To allow the NE levels to reach steady state, the dialysate sampling was started from 120 min after implantation of the dialysis probe. Taking into account the dead space volume between the dialysis membrane and sample tube, dialysate sampling was started.

After interfering compounds in the dialysate were removed by an alumina procedure, we measured NE and EPi concentrations using high-performance liquid chromatography with electrical chemical detection [8,24].

We examined basal dialysate NE levels during administration of ketamine (10 mM). Ringer solution containing ketamine was locally administered through the dialysis probe. We measured the dialysate NE levels at 30-min intervals after the initiation of ketamine administration. The myocardial interstitial NE levels are mainly regulated by exocytotic (dependent on N-type Ca^{2+} channel) NE release and subsequent neuronal NE uptake (sensitive to desipramine) at surrounding cardiac sympathetic nerve endings [25]. To examine the effects of these factors on the ketamine-induced NE increment, neuronal blocking agents on both exocytosis (ω-conotoxin GVIA, 10 μg/kg, i.v.) and membrane NE transport (desipramine, 100 μM) were co-administered. We measured the ketamine-induced dialysate NE response with this pretreatment. The ketamine-induced NE response was expressed as the changes in dialysate NE from the basal level.

Several studies have shown that ketamine exerts a neuroprotective effect in the central nervous system [11,13–15]. We examined whether at the cardiac sympathetic nerve ending, ketamine modulates the ischemia-induced catecholamine release in separate animals. The dialysate NE and EPi responses evoked by 60 min LAD occlusion were measured in the presence and absence of 10 mM ketamine. Further, with the addition of desipramine, the same protocol was performed in the presence and absence of ketamine.

Experimental animals were killed at the end of the experiments with an overdose of pentobarbital sodium. We then verified the position of the dialysis probe in the middle layer of the left ventricular myocardium.

Analysis of variance with repeated measures was applied to analyze differences [23]. When statistical significance was detected, the Tukey procedure was applied. A non-paired *t*-test was performed to compare the dialysate NE levels during coronary occlusion with and without ketamine. Statistical significance was defined as $P < 0.05$. Values are presented as means ± standard error.

Local administration of ketamine did not change heart rate or mean arterial pressure. Ketamine induced increases in dialysate NE levels (Fig. 1). The pretreatment with desipramine and ω-conotoxin GVIA increased basal dialysate NE levels (vehicle, 37 ± 4 pg/ml; pretreatment, 79 ± 5 pg/ml). However, the ketamine-induced increment in dialysate NE was not altered by the addition of desipramine and ω-conotoxin GVIA.

Ketamine induced an increase in the dialysate NE level, which was similar to the level of the dialysate NE response evoked by electrical stimulation of the stellate ganglia at 5 Hz [25]. Generally, exocytotic NE release from the stored vesicle is triggered by Ca^{2+} channel opening. Further, in pathophysiological conditions, the NE transporter runs in the reverse direction due to a reduced Na^{+} gradient and releases NE from the axoplasmic site to the extracellular space [5,18,19]. In either case, addition of ω-conotoxin GVIA and desipramine could suppress exocytotic or non-exocytotic NE release. The ketamine-induced increment in dialysate NE level was not suppressed by the addition of ω-conotoxin GVIA and desipramine. This result suggests that the ketamine-induced increment in dialysate NE was independent of exocytosis or membrane NE transport. ω-Conotoxin GVIA and desipramine insensitive NE efflux was observed under co-administration of a monoamine oxidase inhibitor and a vesicle NE transport inhibitor [26] that leads to the mobilization of NE from the stored NE vesicle and the displacement of NE into the extracellular space. Ketamine may have the property of being able to mobilize vesicle NE

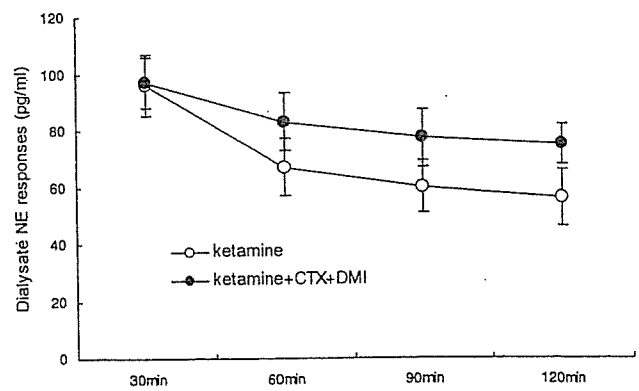

Fig. 1. The time course of ketamine (10 mM)-induced dialysate NE responses with and without pretreatment with ω-conotoxin GIVA (CTX: 10 μg/kg i.v.) and desipramine (DMI: 100 μM). Values are means ± SE (for each group, $n = 5$).

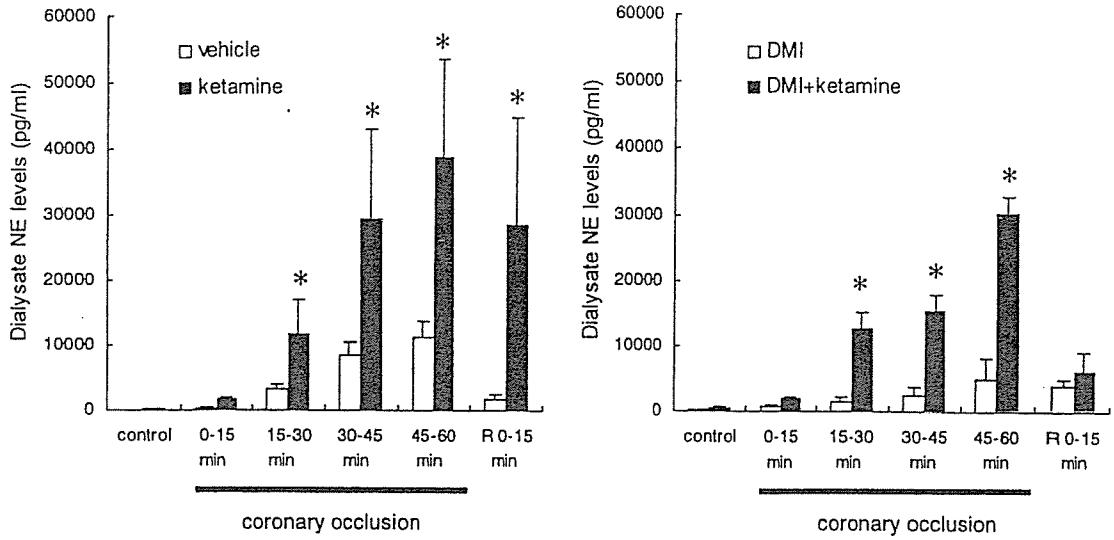

Fig. 2. Left panel: Effect of ketamine (10 mM) on coronary occlusion induced dialysate NE responses. *$P < 0.05$ (vs. vehicle). Right panel: Effect of ketamine (10 mM) on coronary occlusion induced dialysate NE responses with pretreatment of desipramine. *$P < 0.05$ (vs. desipramine group). DMI, desipramine; R, reperfusion. Values are means ± SE (for each group, $n = 6$).

in order to behave as an effective releaser [21] and induce NE efflux through the diffusion rather than NE transport.

Coronary occlusion induced decreases in heart rate and mean arterial pressure. There were no significant differences in hemodynamic changes with or without ketamine. Fig. 2 shows the time course of dialysate NE levels during LAD occlusion. Dialysate NE levels increased gradually and reached peak levels at 45–60 min of occlusion. The addition of ketamine (10 mM) augmented the response of dialysate NE levels to LAD occlusions. The ischemia-induced peak level of dialysate NE was three times higher than that in the vehicle group. Pretreatment with desipramine suppressed the responses of dialysate NE levels to LAD occlusions compared with the vehicle group, whereas the addition of desipramine + ketamine augmented the responses of dialysate NE levels to LAD occlusions compared with the desipramine group.

In hypoxic or ischemic heart, non-exocytotic NE release plays a critical role in NE release from sympathetic nerve endings. Several studies have suggested that non-exocytotic release of NE is required to be a two-step process in the sympathetic nerve endings consisting of axoplasmic NE elevation and outward NE transport [18,19]. Ketamine has been implicated in both of these. From the first experiment, ketamine may be concluded to mobilize vesicle NE into the axoplasma and elevate axoplasmic NE levels. Furthermore, ketamine exerts an inhibitory effect on membrane NE transport [6,20]. If the former effect is the primary mechanism of ketamine's effect on myocardial ischemia, ketamine could augment NE efflux from the ischemic region. Alternatively, if the latter effect is mainly involved in the ischemia, ketamine could suppress NE efflux with inhibition of membrane outward NE transport. Ischemia-induced NE release was not suppressed by ketamine; or rather, ketamine augmented NE release from the cardiac sympathetic nerve endings. Therefore, it is unlikely that ketamine exerts an inhibitory action on membrane NE transport. Our result suggests that ketamine augmented the elevation of the axoplasmic NE level, leading to ketamine-induced NE efflux without interfering with the membrane NE transporter. The pretreatment with desipramine inhibited NE efflux but did not inhibit the ketamine-induced augmentation of NE efflux. This finding also supports the contention that the ketamine-induced increment is not mediated through the neuronal NE transporter.

At the control and early to mid phases of 60-min myocardial ischemia, dialysate Epi was undetectable, whereas dialysate Epi appeared at the late phase of myocardial ischemia (Fig. 3). Ketamine augmented Epi release at this phase.

A study by Schomig et al. indicated the presence of cardiac Epi release in the ischemic rat heart [18]. Further-

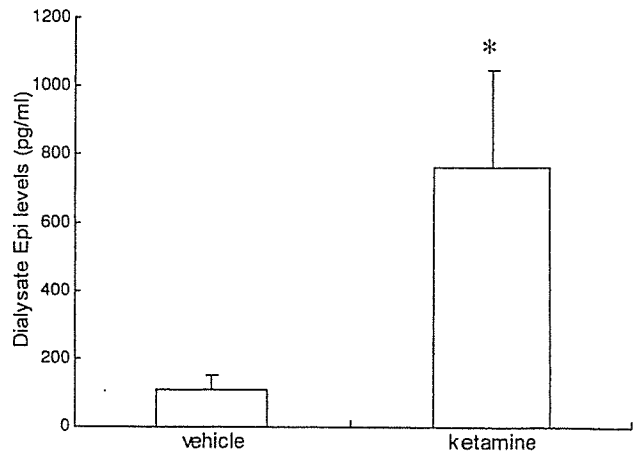

Fig. 3. Effect of ketamine on dialysate Epi levels in response to coronary occlusion. Epi values at 45–60 min of coronary occlusion Values are means ± SE (for each group, $n = 5$). *$P < 0.05$ (vs. vehicle).

more, we examined the effect of chemical hypoxia (induced by cyanide) on cardiac Epi release in the anesthetized rabbit and found that local administration of cyanide caused Epi release in addition to NE release [9,10]. In the present study, myocardial ischemia induced a small amount of Epi release at 45–60 min of coronary occlusion in the anesthetized cat. This EP release was augmented by the addition of ketamine. We did not find Epi release evoked by ketamine in the resting state. It is well known that ketamine reduces the ventricular arrhythmogenic dose of Epi [3,7]. Ketamine itself may induce EP release, which is involved in the occurrence of ventricular arrhythmia during myocardial ischemia.

In conclusion, local administration of ketamine induced an increase in dialysate NE levels, which was insensitive to the N-type Ca^{2+} channel blocker and NE transport inhibitor. Furthermore, we observed that ketamine markedly augmented the NE and Epi efflux evoked by myocardial ischemia. The ketamine-induced NE increment is not mediated through the neuronal NE transporter.

This study was by the program for Promotion of Fundamental Studies in Health Science of the Organization for Pharmaceutical Safety and Research, Health Sciences Research Grant for Advanced Medical Technology from the Ministry of Health and Welfare of Japan, Ground-Based Research Grant for the Space Utilization promoted by NASDA (National Development Agency of Japan) and Japan Space Forum.

[1] Akiyama, T., Yamazaki, T. and Ninomiya, I., In vivo monitoring of myocardial interstitial norepinephrine by dialysis technique, Am. J. Physiol., 261 (1991) H1643–H1647 (Heart Circ. Physiol., 30).
[2] Asai, S., Kohna, T., Katayama, Y., Iribe, Y., Hosoi, I., Kanematsu, K., Kunimatsu, T. and Ishikawa, K., Oxygen-independent real-time monitoring of distinct biphasic glutamate release using dialysis electrode in rat striatum during anoxia: in vivo evaluation of glutamate release and reverse uptake, J. Neurotrauma, 17 (2000) 1105–1114.
[3] Bednarski, R.M., Sams, R.A., Majors, L.J. and Ashcraft, S., Reduction of the ventricular arrhythmogenic dose of epinephrine by ketamine administration in halothane-anesthetized cats, Am. J. Vet. Res., 49 (1988) 350–354.
[4] Cook, D.J., Housmans, P.R. and Rorie, D.K., Effect of ketamine HCl on norepinephrine disposition in isolated ferret ventricular myocardium, J. Pharmacol. Exp. Ther., 261 (1992) 101–107.
[5] Dart, A.M., Riemersma, R.A., Schomig, A. and Ungar, A., Metabolic requirements for release of endogenous noradrenaline during myocardial ischemia and anoxia, Br. J. Pharmacol., 90 (1987) 43–50.
[6] Hara, K., Yanagihara, N., Minami, K., Ueno, S., Toyohira, Y., Sata, T., Kawamura, M., Bruss, M., Bonisch, H., Shigematsu, A. and Izumi, F., Ketamine interacts with the noradrenaline transporter at a site partly overlapping the desipramine binding site, Naunyn-Schmiedeberg's Arch. Pharmacol., 358 (1998) 328–333.
[7] Hikasa, Y., Okabe, C., Takase, K. and Ogasawara, S., Ventricular arrhythmogenic dose of adrenaline during servoflurane, isoflurane, and halothane anaesthesia either with and without ketamine or thiopentone in cats, Res. Vet. ci., 60 (1996) 134–137.
[8] Kawada, T., Yamazaki, T., Akiyama, T., Sato, T., Shishido, T., Sugimachi, M., Inagaki, M., Alexander Jr., J. and Sunagawa, K., Liquid chromatographic determination of myocardial interstitial epinephrine, J. Chromatogr. B Biomed. Sci. Appl., 714 (1998) 375–378.
[9] Kawada, T., Yamazaki, T., Akiyama, T., Sato, T., Shishido, T., Yoshimura, R., Inagaki, M., Tatewaki, T., Sugimachi, M. and Sunagawa, K., Local epinephrine release in the rabbit myocardial interstitium in vivo, J. Auton. Nerv. Syst., 78 (2000) 94–98.
[10] Kawada, T., Yamazaki, T., Akiyama, T., Sato, T., Shishido, T., Inagaki, M., Tatewaki, T., Yanagiya, Y., Sugimachi, M. and Sunagawa, K., Cyanide intoxication induced exocytotic epinephrine release in rabbit myocardium, J. Auton. Nerv. Syst., 80 (2000) 137–141.
[11] Macoux, F.W., Goodrich, J.E. and Dominick, M.A., Ketamine prevents ischemic neuronal injury, Brain Res., 452 (1988) 329–335.
[12] Nicholls, D.G., Proteins, Transmitters and Synapses, Blackwell, Oxford, 1994, pp. 155–185.
[13] Ransom, B.R., Waxman, S.G. and Davis, P.K., Anoxic injury of CNS white matter: protective effect of ketamine, Neurology, 40 (1990) 1399–1403.
[14] Reeker, W., Werner, C., Mollenberg, O., Mielke, L. and Kochs, E., High-dose S(+)-ketamine improves neurological outcome following incomplete cerebral ischemia in rats, Can. J. Anaesth., 47 (2000) 572–578.
[15] Rothman, S.M., Thurston, J.H., Hauhart, R.E., Clark, G.D. and Solomon, J.S., Ketamine protects hippocampal neurons from anoxia in vitro, Neuroscience, 21 (1987) 673–678.
[16] Saegusa, K., Furukawa, Y., Ogiwara, Y. and Chiba, S., Pharmacologic analysis of ketamine-induced cardiac actions in isolated, blood-perfused canine atria, J. Cardiovasc. Pharmacol., 8 (1986) 414–419.
[17] Sakai, F. and Amaha, K., Midazolam and ketamine inhibit glutamate release via a cloned human brain glutamate transporter, Can. J. Anaesth., 47 (2000) 800–806.
[18] Schomig, A., Dart, A.M., Dietz, R., Mayer, E. and Kubler, W., Release of endogenous catecholamines in the ischemic myocardium of the rat. Part A: Locally mediated release, Circ. Res., 55 (1984) 689–701.
[19] Schomig, A., Kurz, T., Richard, G. and Schomig, E., Neuronal sodium homeostasis and axoplasmic amines concentration determine calcium-independent noradrenaline release in normoxic and ischemic rat heart, Circ. Res., 63 (1988) 214–226.
[20] Takara, H., Wada, A., Arita, M., Sumikawa, K. and Izumi, F., Ketamine inhibits 45Ca influx and catecholamine secretion by inhibiting 22Na influx in cultured bovine adrenal medullary cells, Eur. J. Pharmacol., 125 (1986) 217–224.
[21] Trendelenburg, U., Langeloh, A. and Bonisch, H., Mechanism of action of indirectly acting sympathomimetic amines, Blood Vessels, 24 (1987) 261–270.
[22] Waxman, S.G., Ranson, B.R. and Stys, P.K., Non-synaptic mechanisms of Ca^{2+}-mediated injury in CNS white matter, Trends Neurosci., 14 (1991) 461–468.
[23] Winer, B.J., Statistical Principles in Experimental Design, 2nd Edition, McGraw–Hill, New York, 1971.
[24] Yamazaki, T., Akiyama, T. and Shindo, T., Routine high-performance liquid chromatographic determination of myocardial interstitial norepinephrine, J. Chromatogr. B Biomed. Appl., 670 (1995) 328–331.
[25] Yamazaki, T., Akiyama, T., Kitagawa, H., Takauchi, Y., Kawada, T. and Sunagawa, K., A new, concise dialysis

approach to assessment of cardiac sympathetic nerve terminal abnormalities, Am. J. Physiol., 272 (1997) H1182–H1187.
[26] Yamazaki, T., Kawada, T., Akiyama, T., Kitagawa, H., Takauchi, Y., Yahagi, N. and Sunagawa, K., omega-Conotoxin GVIA and desipramine insensitive norepinephrine efflux from cardiac sympathetic nerve terminal, Brain Res., 761 (1997) 329–332.
[27] Zhan, R.Z., Qi, S., Wu, C., Fujihara, H., Taga, K. and Shimoji, K., Intravenous anesthetics differentially reduce neurotransmission damage caused by oxygen–glucose deprivation in rat hippocampal slices in correlation with *N*-methyl-D-asparate receptor inhibition, Crit. Care Med., 29 (2001) 808–813.
[28] Zhou, Z.S. and Zhao, Z.Q., Ketamine blockage of both tetrodotoxin (TTX)-sensitive and TTX-resistant sodium channels of rat dorsal root ganglion, Brain Res. Bull., 52 (2000) 427–433.

Development of Novel EDG3 Antagonists Using a 3D Database Search and Their Structure−Activity Relationships

Yuuki Koide,*,†,‡ Takeshi Hasegawa,§ Atsuo Takahashi,† Akira Endo,|| Naoki Mochizuki,|| Masako Nakagawa,‡ and Atsushi Nishida*,‡

Drug Research Department, Tokyo Research Laboratories, TOA EIYO Ltd., 2-293-3 Amanuma, Saitama 330-0834, Japan, Graduate School of Pharmaceutical Sciences, Chiba University, 1-33 Yayoicho, Inage, Chiba 263-8522, Japan, Drug Research Department, Fukushima Research Laboratories, TOA EIYO Ltd., 1 Tanaka, Yuno, Iizaka, Fukushima 960-0280, Japan, and Department of Structural Analysis, National Cardiovascular Center Research Institute, 5-7-1 Fujishirodai, Suita, Osaka 565-8565, Japan

Received February 19, 2002

Sphingosine-1-phosphate (S1P) is an intracellular second messenger and an extracellular mediator through endothelial differentiation gene (EDG) receptors, which are a novel class of G-protein-coupled receptors. Although EDG has attracted much attention because of its various roles, no selective agonists or antagonists have yet been developed. This could account for the delay in clarifying the physiological roles of members of the EDG family. Because precise structural information on EDG receptors is not yet available, pharmacophore models were generated based on structural information for S1P using the rational drug design software Catalyst. Novel antagonists, 2-alkylthiazolidine-4-carboxylic acids, were retrieved from a three-dimensional database search using the pharmacophore models, and these showed activity for EDG3. On the basis of their nonphosphoric acid structure, more potent antagonists, 2-(*m*- or *p*-heptylphenyl)thiazolidine-4-carboxylic acid, were developed.

Introduction

Sphingosine-1-phosphate (S1P) is a bioactive lipid mediator that has recently been identified as an intracellular second messenger and an extracellular mediator through endothelial differentiation gene (EDG) receptors, which are a novel class of G-protein-coupled receptors (GPCRs).[1−4] Eight subfamilies of EDG have been identified and among them EDG1, 3, 5, 6, and 8 respond principally to S1P. On the other hand, EDG2, 4, and 7 are activated principally by lysophosphatidic acid (LPA).[5−11] Multiple cellular responses to S1P through EDG, including Ca^{2+} mobilization, modulation of adenylyl cyclase, activation of extracellular signal-regulated kinase (ERK), and mitogen-activated protein kinase (MAPK), have been revealed by many pathological and biological studies.[12−14] On the basis of studies of their mitogenic potential through EDG1, 3, and/or 5, S1P antagonists are expected to be effective therapeutic agents for cardiovascular disease and angiogenesis caused by mitogenic cell growth.[15−18]

Suramin is the only reported antagonist of EDG3 and native LPA receptors.[19−21] However, it is not specific for EDG, and various biological activities, such as adenosine 5′-triphosphate (ATP) receptor antagonism,[22,23] cellular DNA primase inhibition,[24] transforming growth factor α (TGF α) inhibition,[25] and fibroblast growth factor (FGF) antagonism,[26] have been reported. Suramin has also been used as a therapeutic agent for filariasis.[27] Because of its multiple biological activities, suramin is not suitable for studying the pathological functions of EDG.

We searched for a novel and specific EDG1 and/or EDG3 antagonist, which might be suitable as a therapeutic agent for promoting angiogenesis and the proliferation and migration of endothelial cells by the rational drug design approach. A recent study using homology modeling showed three interactions between EDG1 and S1P.[28,29] Considering this structural information, we generated Catalyst pharmacophore models,[30] which are called hypothesis models in Catalyst, for an EDG ligand based on the structure of S1P and searched a three-dimensional (3D) database. Two novel compounds were retrieved from the 3D database,[31] and these showed antagonist activity using Hela cells that overexpressed EDG3.[32] In this paper, we report these novel and effective EDG3 antagonists and their structure−activity relationships.

Results and Discussion

Because S1P has a flexible long alkyl chain, it is difficult to determine its active conformation. Therefore, we generated multiple conformations that should be able to cover the entire conformational space of S1P by Catalyst conformer generation using the Poling method.[33−35] Twenty conformations of S1P within ΔE = 3 kcal mol^{-1} from the minimum energy conformer were chosen.

These conformations were manually transferred into hypothesis models. A homology study suggested interaction between two cationic amino acids, Arg^{120} and Arg^{292}, and the phosphoric acid of S1P with EDG1.[28,29] Furthermore, Glu^{121} was expected to interact with an amino group of S1P. These residues were conserved

* To whom correspondence should be addressed. Y.K.: Tel: +81-(48)6477971. Fax: +81(48)6480078. E-mail: koide.yuuki@toaeiyo.co.jp. A.N.: Tel: +81(43)2902907. Fax: +81(43)2902909. E-mail: nishida@p.chiba-u.ac.jp.
† Tokyo Research Laboratories, TOA EIYO Ltd..
‡ Chiba University.
§ Fukushima Research Laboratories, TOA EIYO Ltd..
|| National Cardiovascular Center Research Institute.

10.1021/jm020080c CCC: $22.00
Published on Web 09/13/2002

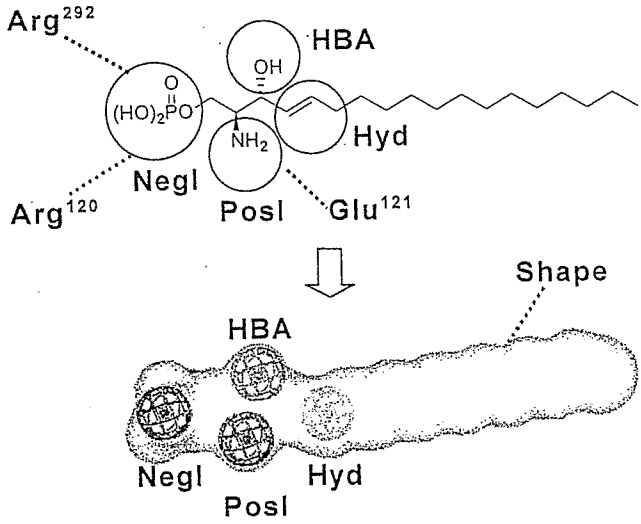

Figure 1. Generation of Catalyst hypothesis models.

among EDG1, EDG3 (Arg^{114}, Glu^{115}, and Lys^{279}), and EDG 5 (Arg^{108}, Glu^{109}, and Lys^{269}). These three interactions could be represented as a positive ionizable feature (PosI) and negative ionizable feature (NegI) in the Catalyst default feature as a blob with 1.5 Å of tolerance (Figure 1). Because 4,5-dihydro-S1P (DHS1P) was less potent than S1P in cells that overexpressed S1P responsive EDGs,[36] the double bond should be important for binding to S1P responsive EDGs. Thus, we made the double bond of S1P a hydrophobic feature (Hyd). The role of the secondary hydroxyl group of S1P is not yet clear. However, EDG1 and EDG2 can differentiate between S1P and LPA. Therefore, we made the hydroxyl group a hydrogen acceptor feature (HBA). Furthermore, we added a shape feature that describes the molecular volume to within a tolerance of 70−130%. Thus, our hypothesis model consisted of five features: PosI, NegI, Hyd, HBA, and shape. Twenty hypothesis models were generated from 20 conformations (Figure 2). They could be classified into four clusters: straight (S), spherical (SP), bent (B), and extremely bent (EB), according to their shape. Commercially available compounds in the Available Chemical Directory (ACD) database[37] were searched using these hypothesis models as a 3D query. Fifty-eight hit compounds were retrieved from the ACD database. Among the four clusters, the SP cluster gave the most hit compounds. In contrast, no hit compounds were found in the EB cluster.

Thirty-two of the hit compounds (Figure 3), excluding S1P, were evaluated for their ability to inhibit the S1P-induced rapid and transient increase in $[Ca^{2+}]_i$ in Hela cells that overexpressed EDG1 or EDG3 (Hela-EDG1 or Hela-EDG3).[32] We defined compounds that produced inhibition of more than 30% as active. Two compounds, 2-alkylthiazolidine-4-carboxylic acids (**1** and **2**, Maybridge Chemical Co., Ltd., RH00666 and RH00669), showed more than 30% inhibition at 10 μM as EDG3 antagonists and did not increase $[Ca^{2+}]_i$ by themselves. They were also suitable for further optimization as antagonists because of their unique nonphosphoric structure and low molecular weight as compared to

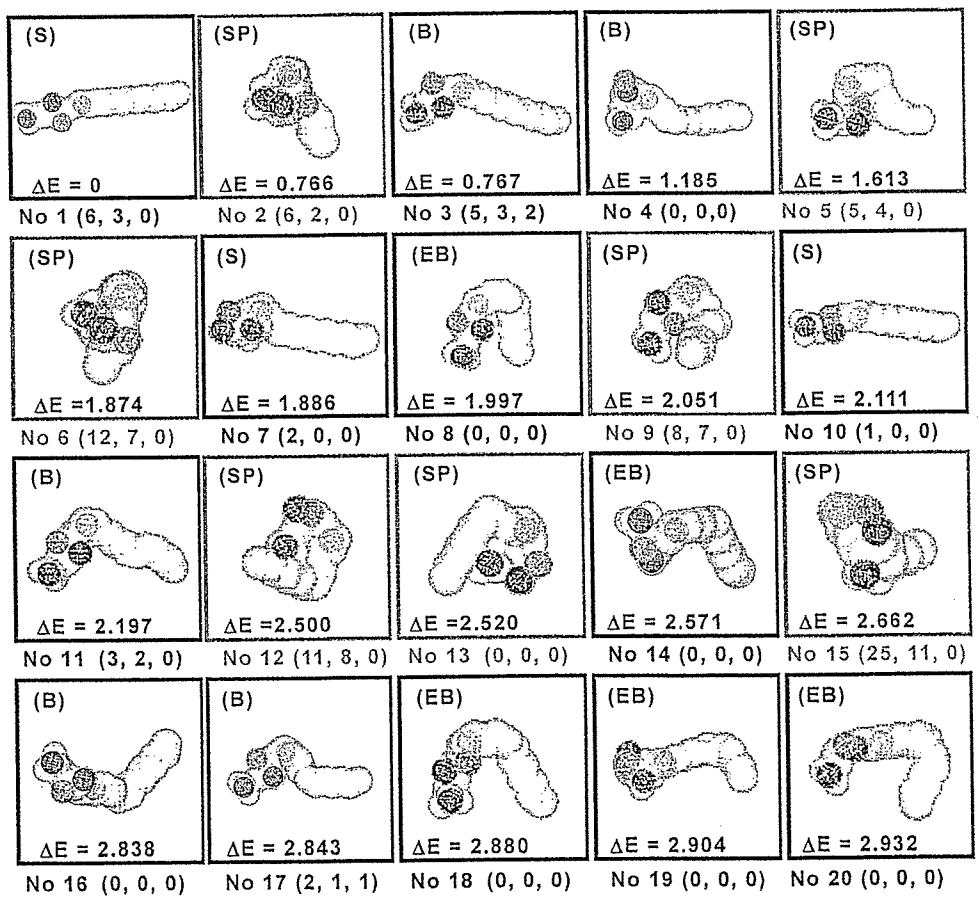

Figure 2. Manually generated Catalyst hypothesis models of S1P. Number of hit compounds, number of tested compounds, and number of active compounds are in parentheses. S, straight conformation; SP, spherical conformation; B, bent conformation; EB, extremely bent conformation. ΔE (kcal mol^{-1}) means the difference in energy from a minimum energy conformer.

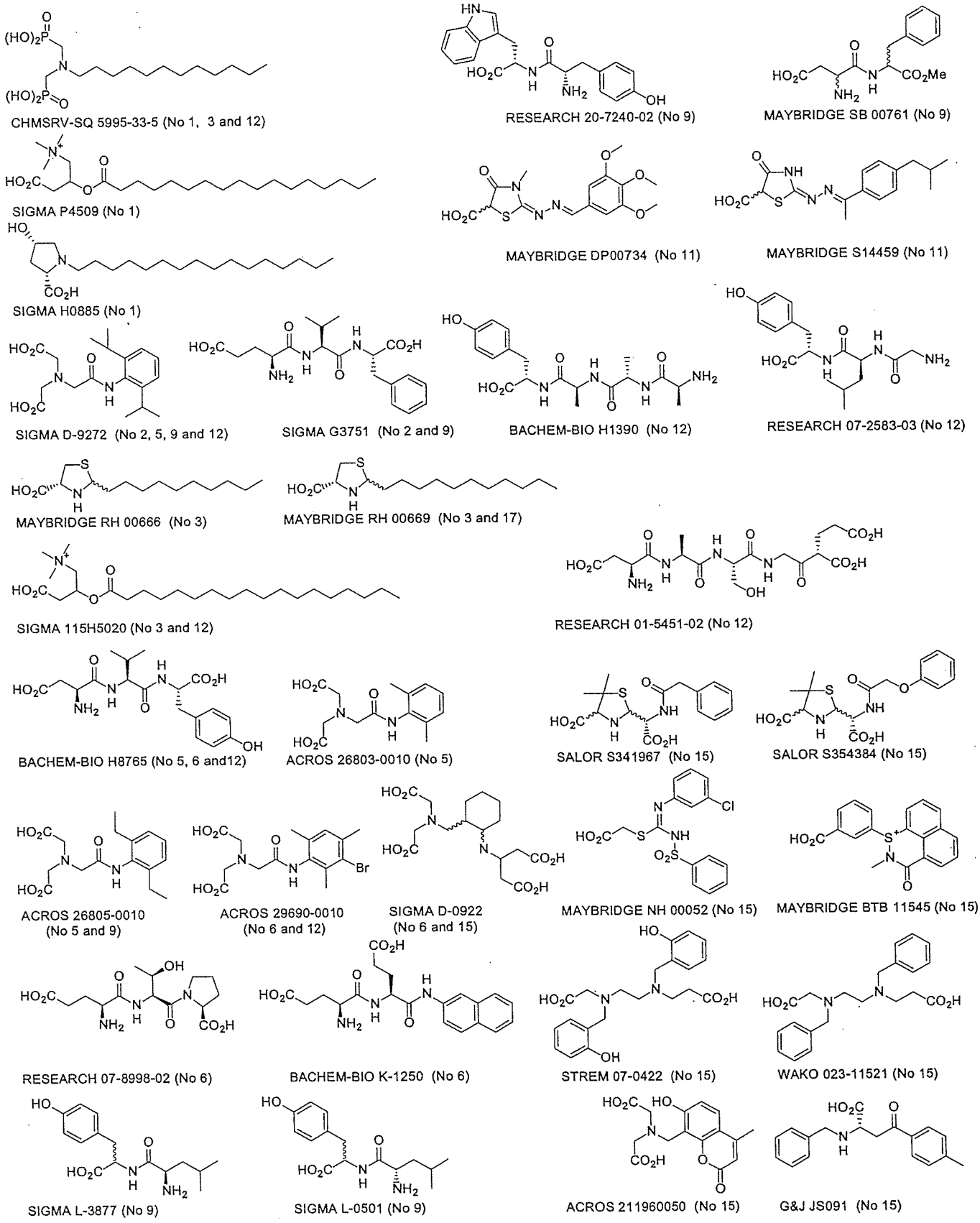

Figure 3. Structures of assayed compounds registered in the ACD99 database. Numbers in parentheses show the hypothesis model that hit the compound.

suramin. According to a ^{1}H NMR study, they were a 1:1 mixture of diastereomers due to a C2 stereogenic center with an (*R*)-configuration at C4.

They were obtained using hypothesis model Nos. 3 and 17, which were classified as cluster B. We assumed that an antagonist would bind the EDG receptor in

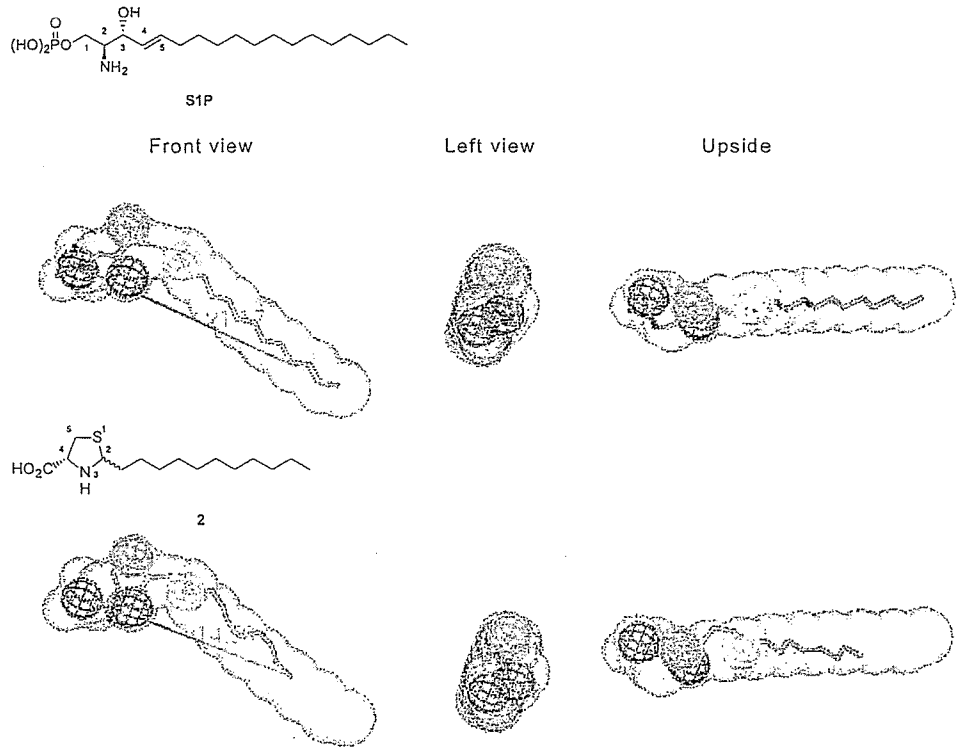

Figure 4. Comparison of two active conformations, S1P and 2-undecyl thiazolidine-4-carboxylic acid **2**, superimposed on hypothesis No. 3.

almost the same fashion as the agonist S1P and that the antagonist would lack a critical functional group to cause agonist activity. Although it is not yet known why compounds **1** and **2** show antagonist activity, it may be worth considering several structural features of **2**. The slightly bent conformation of S1P is mainly determined by the dihedral angle of C2−C3−C4−C5, while the related conformation of **2** is governed by the dihedral angle of S1−C2−C6−C7. Compound **2** (14.59 Å) is shorter than S1P (21.17 Å). A difference in electron density at the head part between S1P and **2** might be critical for their difference in activity. Compound **2** was superimposed on hypothesis model No. 3 to compare the active conformations (Figure 4).

Four derivatives, **3**−**6**, were synthesized by known methods to clarify the effect of the molecular length of **2** on its inhibitory activity.[38] We also prepared a stereoisomer **7**, which has an opposite stereocenter at C4, from D-cysteine (Scheme 1). In addition, five racemic thiazinane derivatives, **8**−**12**, were also synthesized.

The lower activity of DHS1P as compared to S1P as a ligand for EDG suggests that the double bond in the chain may play an important role.[36] Although a higher activity was expected with the introduction of a trans double bond at a suitable position in **2**, difficulties in preparing these analogues prompted us to focus on new analogues, **19**−**24**, with an *m*- or *p*-alkylated phenyl ring (Schemes 2 and 3). Recently, it has been reported that the double bond of sphingolipid could be substituted by an *m*- or *p*-alkylated phenyl group.[39] These 18 derivatives were assayed using Hela-EDG1 or Hela-EDG3 cells (Figure 5).

With regard to the alkyl side chain, compound **2**, which has an undecyl group, showed the most potent inhibitory effects in a series of thiazolidine derivatives, **3**−**6**. Five-membered thiazolidine derivatives were superior to derivatives of six-membered thiazinane. Compound **7**, which has a (4*S*) configuration and is a stereoisomer of **1**, was less potent than **1**, which has a (4*R*) configuration. 2-(*m* or *p*-Heptylphenyl)thiazolidine-4-carboxylic acids **20** and **23** had the most potent inhibitory effects. Suramin did not have any effect in our assay system. Furthermore, we did not find any compound with obvious inhibitory activity in Hela-EDG1.

Scheme 1. Preparation of 2-Alkylated Thiazolidine and [1,3]Thiazinane-4-carboxylic Acid Derivatives

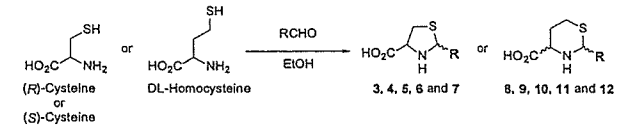

compd	substrate	R	yield (%)
3	(*R*)-Cysteine	*n*-C_6H_{13}	49[a]
4	(*R*)-Cysteine	*n*-C_9H_{19}	69[a]
5	(*R*)-Cysteine	*n*-$C_{12}H_{33}$	71[a]
6	(*R*)-Cysteine	*n*-$C_{13}H_{27}$	73[a]
7	(*S*)-Cysteine	*n*-$C_{10}H_{21}$	60[a]
8	DL-Homocysteine	*n*-C_9H_{19}	60[b]
9	DL-Homocysteine	*n*-$C_{10}H_{21}$	53[b]
10	DL-Homocysteine	*n*-$C_{11}H_{23}$	71[b]
11	DL-Homocysteine	*n*-$C_{12}H_{25}$	71[b]
12	DL-Homocysteine	*n*-$C_{13}H_{27}$	56[b]

[a] Conditions: EtOH, room temperature, 1 h. [b] Conditions: EtOH−H_2O, reflux, 12 h.

Compounds **3** and **4**, which have a side chain of fewer than 10 carbons, were less active than compound **1**. We merged the new hydrophobic feature (Hyd-2) into hypothesis model No. 3 to describe this important hydrophobic interaction (Figure 6A). Compounds **2**, **20**, and **23** were superimposed on this model (Figure 6B). The relative energies of each conformation that fit hypothesis model No. 3′ were 11.7113 kcal mol^{-1} (**2**), 16.0002 kcal mol^{-1} (**20**), and 9.497 76 kcal mol^{-1} (**23**).

Scheme 2. Synthesis of *m*- or *p*-Substituted Benzaldehyde[a]

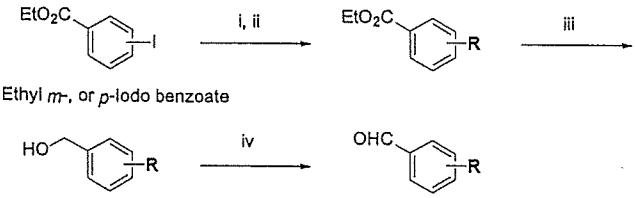

compd	R	yield (%)
13	*m*-(*n*-C_5H_{11})	26
14	*m*-(*n*-C_7H_{15})	37
15	*m*-(*n*-C_9H_{19})	33
16	*p*-(*n*-C_5H_{11})	29
17	*p*-(*n*-C_7H_{15})	27
18	*p*-(*n*-C_9H_{19})	24

[a] Reaction conditions: (i) alkyne, $PdCl_2(PPh_3)_2$, CuI, *i*Pr_2NH, CH_3CN, room temperature, 12 h. (ii) H_2, Pd−C, EtOH, room temperature, 12 h. (iii) $LiAlH_4$, Et_2O, room temperature, 1 h. (iv) MnO_2, $CHCl_3$, room temperature, 2 h.

Scheme 3. Preparation of 2-(*m*- or *p*-alkylated)phenyl-4-carboxylic Acid Derivatives[a]

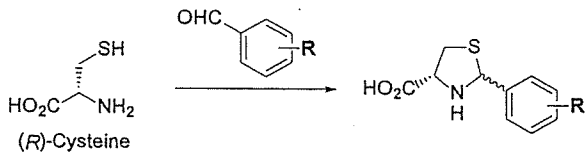

compd	R	yield (%)
19	*m*-(*n*-C_5H_{11})	40
20	*m*-(*n*-C_7H_{15})	50
21	*m*-(*n*-C_9H_{19})	62
22	*p*-(*n*-C_5H_{11})	60
23	*p*-(*n*-C_7H_{15})	77
24	*p*-(*n*-C_9H_{19})	45

[a] Conditions: EtOH, room temperature, 12 h.

We estimated the affinity of these derivatives by fit values, which reflect the quality of mapping in a hypothesis model. [40] Fit values were calculated for each optical isomer of all derivatives and adjusted by considering the ratio of diastereomers, since the assay was performed using a mixture of isomers (Table 1). The fit values of thiazolidine derivatives (**1**−**7** and **19**−**24**) were calculated as a 1:1 mixture of diastereomers as determined by ^1H NMR study. In thiazinane derivatives (**8**−**12**), nuclear Overhauser effects (NOE) revealed that the major isomers of thiazinane were (2*R*,4*S*) and (2*S*,4*R*). The ratios of diastereomers and enantiomers of thiazinane derivatives were determined to be 7:3 and 1:1, respectively.

The fit values showed good correlations except for compounds with a side chain longer than compound **2**. Further optimization of the hypothesis model is underway.

Conclusion

We generated multiple hypothesis models based on the conformations of S1P. They were used in a 3D query to search a 3D database. Among the 32 compounds assayed, two molecules, 2-alkylthiazolidine-4-carboxylic acids **1** and **2**, showed activity as EDG3 antagonists. These antagonists have a nonphosphoric acid structure with a bent conformation. Further structure optimization led to 2-(*m*-heptylphenyl)thiazolidine-4-carboxylic acid **20**, which may be a new lead compound for the development of therapeutic agents.

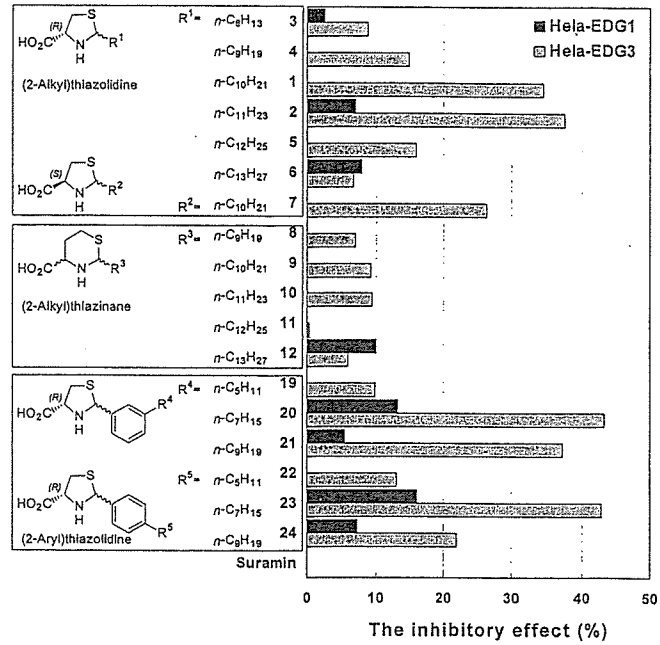

Figure 5. Inhibitory effects of the test compounds (10 μM) on EDG1 and EDG3. The inhibitory effect (%) of the test compound (10 μM) on the S1P (1 μM)-induced increase in $[Ca^{2+}]_i$ in Hela-EDG cells was observed as a difference in RFU from the control.

Experimental Section

Materials. S1P was purchased from SIGMA and solubilized to 10^{-2} M in dimethyl sulfoxide (DMSO). Dulbecco's modified Eagle's medium (DMEM), Dulbecco's phosphate-buffered saline (+) (D-PBS (+)), and fetal bovine serum (FBS) were also purchased from SIGMA. Minimum essential medium was purchased from GIBCO BRL. The fluorescence reagent Calcium Green-1 AM was purchased from Molecular Probes.

Measurement of $[Ca^{2+}]_i$ Inhibition. Cloned cells expressing EDG1 or **3** (Hela-EDG1 cells or Hela-EDG3 cells) were obtained by transfection of Hela cells with human cDNA of EDG1 or EDG3. Inhibition of the S1P-induced cytoplasmic free calcium concentration ($[Ca^{2+}]_i$) in each cell by each antagonist was measured as described below. Suspensions of Hela-EDG cells in DMEM containing 10% (v/v) FBS were loaded on 96 well plates (approximately 1×10^5 cells/well). After they were incubated for 24 h at 37 °C, the cells were washed once with DMEM and then incubated in MEM for 24 h at 37 °C. Cells were washed twice with D-PBS (+) and then maintained with D-PBS (+) containing 5 μM fluorescence reagent Calcium Green-1 AM for 60 min at 37 °C. Cells were washed twice with D-PBS (+). After the cells were maintained with D-PBS (+) for 25 min at 37 °C, they were treated with D-PBS (+) containing 10 μM test compound and incubated for 5 min at 37 °C. After 1 μM S1P was added, fluorescence (excitation at 485 nm; emission at 535 nm) was immediately measured for 30 s at intervals of 3 s with a Fluorescence Ascent FL fluorescence spectrometer (Labsystems). Inhibition was observed as a difference in relative fluorescence units (RFU) between the control, the D-PBS (+) containing 0.1% DMSO, and the test compound. The inhibitory activity was calculated as the average of three wells on the same plate. This experiment was repeated three times on different days, and the inhibitory profiles of the test compounds were identical.

Computational Methods. This study was performed using the software package Catalyst 4.6 (Accelrys Inc., San Diego,

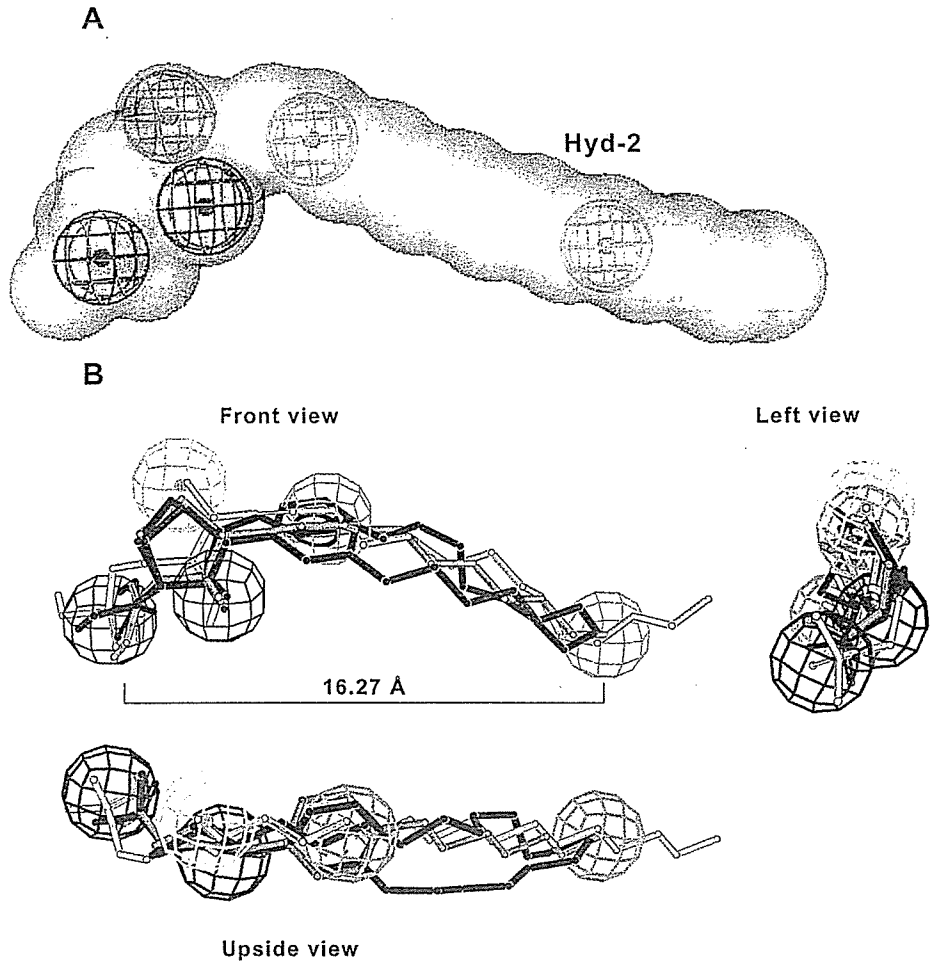

Figure 6. Hypothesis model No. 3′ of S1P and its superimposition. (A) Hypothesis model No. 3′, which incorporated the new hydrophobic feature (Hyd-2). (B) Superimposition of compounds **2**, **20**, and **23**. The shape feature is not shown to clarify the superimposed structures.

Table 1. Fit Values for Each Compound Using Hypothesis Model No. 3′[a]

	compd	4*R*,2*R*	4*R*,2*S*	4*S*,2*R*	4*S*,2*S*	avg of fit value	inhibitory effect (%)
3	$R^1 = n\text{-}C_6H_{13}$	0	0			0	0
4	$n\text{-}C_9H_{19}$	2.972 61	0			1.486 31	14.8
1	$n\text{-}C_{10}H_{21}$	3.980 81	3.617 60			3.799 21	34.5
2	$n\text{-}C_{11}H_{23}$	4.148 84	4.146 01			4.147 43	37.6
5	$n\text{-}C_{12}H_{25}$	4.327 97	4.133 71			4.230 84	15.9
6	$n\text{-}C_{13}H_{27}$	4.143 19	4.266 10			4.204 65	6.6
7	$R^2 = n\text{-}C_{10}H_{21}$			3.657 59	3.561 35	3.609 47	26.4
8	$R^3 = n\text{-}C_9H_{19}$	0	0	1.751 16	2.102 86	0.928 34	6.9
9	$n\text{-}C_{10}H_{21}$	0	3.547 35	3.423 95	3.896 10	3.024 37	9.3
10	$n\text{-}C_{11}H_{23}$	3.693 91	3.894 07	3.130 57	4.422 34	3.676 06	9.4
11	$n\text{-}C_{12}H_{25}$	2.720 14	4.114 95	3.524 18	3.137 55	3.552 35	0.3
12	$n\text{-}C_{13}H_{27}$	3.723 02	3.991 27	3.878 61	4.610 82	4.004 53	5.9
19	$R^4 = n\text{-}C_5H_{11}$	0	0			0	9.9
20	$n\text{-}C_7H_{15}$	3.890 05	3.420 23			3.655 14	43.4
21	$n\text{-}C_9H_{19}$	4.110 05	3.334 08			3.722 07	37.2
22	$R^5 = n\text{-}C_5H_{11}$	2.673 94	0			1.336 97	13.0
23	$n\text{-}C_7H_{15}$	4.378 12	3.843 41			4.110 77	42.9
24	$n\text{-}C_9H_{19}$	4.250 51	4.331 90			4.291 21	21.9

[a] Absolute ring configurations are described. Data on the inhibitory effect are the same as those in Figure 5.

CA). All calculations were conducted on an SGI Octane (R 8000), running under the IRIX 6.5.4 operating system. Conformational models for S1P were calculated using a 16 kcal mol^{-1} energy cutoff for the "best quality" conformational search option. Conformational models for other compounds were calculated using a 20 kcal mol^{-1} energy cutoff for the best quality. The number of conformers generated for each molecule was limited to a maximum of 255 and ensured maximum coverage in the conformational space. A hypothesis model consisted of HBA, Hyd, positive ionizable (PosI), negative ionizable (NegI), and shape features, as shown in Figure 2. The shape feature had a tolerance of within 70−130% of molecular volume similarity, and other blob features had a tolerance of 1.5 Å. To compare and fit a compound with a hypothesis model, the best fit mode was selected.

Chemistry. General Information. Melting points were determined with a Yanako MP-500V micromelting point apparatus (uncorrected), and ^1H and ^{13}C NMR spectra were recorded on a JEOL JNM-AL-300, using $CDCl_3$, CD_3OD, or DMSO-d_6 as solvents, with Me_4Si as an internal standard.

Mass spectra were recorded on either a JEOL HX-110A (FAB) or Finnigan LCQ (ESI). Elemental analyses were performed by Toray Research Center, Inc. Reactions were monitored by TLC analysis using E. Merck silica gel $60F_{254}$ thin layer plates. Flash chromatography was carried out on E. Merck Kieselgel 60 (230−400 mesh) silica gel. Thirteen thiazolidine derivatives, **1**−**7** and **19**−**24**, were reported as diastereomeric mixtures [(2*R*,4*R*) and (2*S*,4*R*)]. Five thiazinane derivatives, **8**−**12**, were racemic and were reported as diastereomeric mixtures [(2*R**,4*R**) and (2*S**,4*R**)].

***m*-Pentylbenzaldehyde (13).** To a solution of ethyl 3-iodobenzoate (5.29 g, 19.16 mmol) in CH_3CN (50 mL) were added 1-pentyne (1.9 mL, 14.12 mmol), diisopropylamine (2.5 mL, 17.66 mmol), dichlorobis(triphenylphosphine)palladium (83 mg, 0.12 mmol), and copper iodide (45 mg, 0.24 mmol) at 0 °C. The mixture was stirred for 12 h, diluted with Et_2O, washed sequentially with 5% $KHSO_4$, 5% $Na_2S_2O_3$, and brine, dried over Na_2SO_4, filtered, and concentrated. Column chromatography (100:1 hexane:Et_2O) provided *m*-(1-pentynyl)-benzoic acid ethyl ester as an orange oil.

The oil was dissolved in EtOH (25 mL), and 10% Pd/C was added (0.53 g). A balloon of hydrogen gas was attached, and the reaction was stirred rapidly for 12 h, filtered through a pad of Celite, and concentrated. Short column chromatography (100:1 hexane:AcOEt) provided *m*-pentylbenzoic acid ethyl ester as a yellow oil.

After the ester was dissolved in Et_2O (100 mL), the solution was added dropwise into a suspension of lithium aluminum hydride (471 mg, 12.40 mmol) in Et_2O (50 mL) over more than 15 min. The reaction was stirred for 2 h at 0 °C, diluted with Et_2O (50 mL), and quenched with MeOH (5 mL). Saturated Rochelle salt (50 mL) was then added to the mixture and stirred for 1 h. The product was extracted with Et_2O, and the ether solution was washed with brine, dried over Na_2SO_4, filtered, and concentrated. Column chromatography (100:1 hexane:AcOEt) provided *m*-pentylbenzyl alcohol as a pale yellow oil.

The alcohol was dissolved in CH_2Cl_2 (50 mL), and activated manganese oxide was added (WAKO Pure Chemical Industries, Ltd.) (5.90 g, 67.85 mmol). The mixture was stirred for 2 h, manganese oxide was filtered off through a pad of Celite, and the filtrate was concentrated. Column chromatography (100:1 hexane:Et_2O) provided compound **13** as a colorless oil (886 mg, 5.03 mmol, 26% from ethyl 3-iodobenzoate). ^{1}H NMR (300 MHz, $CDCl_3$): δ 10.00 (s, 1H, CHO), 7.70−7.68 (m, 2H, 2, 5-ArH), 7.45−7.43 (m, 2H, 4, 6-ArH), 2.68 (t, J = 7.52 Hz, 2H, 1′-CH_2), 1.70−1.62 (m, 2H, 2′-CH_2), 1.40−1.31 (m, 4H, CH_2), 0.90 (t, J = 6.97 Hz, 3H, 5′-CH_3). ^{13}C NMR (75 MHz, $CDCl_3$): δ 192.67 (CHO), 143.96 (C3), 136.49 (C1), 134.72 (C4), 129.32 (C2), 128.87 (C5), 127.51 (C6), 35.59 (C1′), 31.37 (C2′), 30.94 (C3′), 22.47 (C4′), 13.98 (C5′). MS (FAB): *m/z* 177 (MH^+). HRMS (FAB) calcd for $C_{12}H_{17}O$ (MH^+), 177.2628; found, 177.1264.

***m*-Heptylbenzaldehyde (14).** Compound **14** was prepared according to the procedure described for **13** but using 1-heptyne instead of 1-pentyne. Compound **14** was obtained as a colorless oil (953 mg, 4.67 mmol, 37% from ethyl 3-iodobenzoate). ^{1}H NMR (300 MHz, $CDCl_3$): δ 10.01 (s, 1H, CHO), 7.71−7.70 (m, 2H, 2, 5-ArH), 7.45−7.43 (m, 2H, 4, 6-ArH), 2.68 (t, J = 7.34 Hz, 2H, 1′-CH_2), 1.67−1.59 (m, 2H, 2′-CH_2), 1.42−1.28 (m, 8H, CH_2), 0.88 (t, J = 6.24 Hz, 3H, 7′-CH_3). ^{13}C NMR (75 MHz, $CDCl_3$): δ 192.68 (CHO), 143.99 (C3), 136.50 (C1), 134.72 (C4), 129.33 (C2), 128.88 (C5), 127.50 (C6), 35.63 (C1′), 31.75 (C2′), 31.27, 29.17, 29.11, 22.64 (C6′), 14.81 (C7′). MS (FAB) *m/z* 205 (MH^+). HRMS (FAB) calcd for $C_{14}H_{21}O$ (MH^+), 205.3159; found, 205.1591.

***m*-Nonylbenzaldehyde (15).** Compound **15** was prepared according to the procedure described for **13** but using 1-nonyne instead of 1-pentyne. Compound **15** was obtained as a colorless oil (1.31 g, 5.63 mmol, 33% from ethyl 3-iodobenzoate). ^{1}H NMR (300 MHz, $CDCl_3$): δ 10.00 (s, 1H, CHO), 7.84−7.83 (m, 2H, 2, 5-ArH), 7.69−7.68 (m, 2H, 4, 6-ArH), 2.68 (t, J = 7.42 Hz, 2H, 1′-CH_2), 1.68−1.58 (m, 2H, 2′-CH_2), 1.30−1.24 (m, 12H, CH_2), 0.88 (t, J = 6.79 Hz, 3H, 9′-CH_3). ^{13}C NMR (75 MHz, $CDCl_3$): δ 192.63 (CHO), 143.96 (C3), 136.49 (C1), 134.69 (C4), 129.31 (C2), 128.86 (C5), 127.47 (C6), 35.61 (C1′), 31.84 (C2′), 31.24, 29.48, 29.42, 29.27, 29.19, 22.64 (C8′), 14.08 (C9′). MS (FAB) *m/z* 232 (M^+). HRMS (FAB) calcd for $C_{16}H_{24}O$ (M^+), 232.3612; found, 232.1774.

***p*-Pentylbenzaldehyde (16).** Compound **16** was prepared according to the procedure described for **13** but using ethyl 4-iodobenzoate instead of ethyl 3-iodobenzoate. Compound **16** was obtained as a colorless oil (605 mg, 3.44 mmol, 29% from ethyl 4-iodobenzoate). ^{1}H NMR (300 MHz, $CDCl_3$): δ 9.97 (s, 1H, CHO), 7.79 (d, J = 8.08 Hz, 2H, 2, 6-ArH), 7.33 (d, J = 8.08 Hz, 2H, 3, 5-ArH), 2.68 (t, J = 7.89 Hz, 2H, 1′-CH_2), 1.66−1.59 (m, 2H, 2′-CH_2), 1.32−1.21 (m, 8H, CH_2), 0.88 (t, J = 6.79 Hz, 3H, 7′-CH_3). ^{13}C NMR (75 MHz, $CDCl_3$): δ 192.06 (CHO), 150.52 (C4), 134.36 (C1), 129.89 (C2, 6), 129.07 (C3, 5), 36.16 (C1′), 31.41 (C2′), 30.75 (C3′), 22.47 (C4′), 13.96 (C5′). MS (FAB) *m/z* 176 (M^+). HRMS (FAB) calcd for $C_{12}H_{16}O$ (M^+), 176.1201; found, 176.1193.

***p*-Heptylbenzaldehyde (17).** Compound **17** was prepared according to the procedure described for **16** but using 1-heptyne instead of 1-pentyne. Compound **17** was obtained as a colorless oil (636 mg, 3.12 mmol, 27% from ethyl 4-iodobenzoate). ^{1}H NMR (300 MHz, $CDCl_3$): δ 9.97 (s, 1H, CHO), 7.79 (d, J = 7.89 Hz, 2H, 2, 6-ArH), 7.33 (d, J = 7.89 Hz, 2H, 3, 5-ArH), 2.71−2.66 (t, J = 7.52 Hz, 2H, 1′-CH_2), 1.67−1.60 (m, 2H, 2′-CH_2), 1.35−1.30 (m, 4H, CH_2), 0.90 (t, J = 6.79 Hz, 3H, 7′-CH_3). ^{13}C NMR (75 MHz, $CDCl_3$): δ 192.04 (CHO), 150.49 (C4), 134.36 (C1), 129.88 (C2, 6), 129.06 (C3, 5), 36.21 (C1′), 31.75 (C2′), 31.08, 29.21, 29.10, 22.62 (C6′), 13.96 (C7′). MS (FAB) *m/z* 205 (MH^+). HRMS (FAB) calcd for $C_{14}H_{21}O$ (MH^+), 205.1592; found, 205.1585.

***p*-Nonylbenzaldehyde (18).** Compound **18** was prepared according to the procedure described for **16** but using 1-nonyne instead of 1-pentyne. Compound **18** was obtained as a colorless oil (573 mg, 2.47 mmol, 24% from ethyl 4-iodobenzoate). ^{1}H NMR (300 MHz, $CDCl_3$): δ 9.97 (s, 1H, CHO), 7.79 (d, J = 7.89 Hz, 2H, 2, 6-ArH), 7.33 (d, J = 7.89 Hz, 2H, 3, 5-ArH), 2.68 (t, J = 7.52 Hz, 2H, 1′-CH_2), 1.64−1.56 (m, 2H, 2′-CH_2), 1.30−1.26 (m, 12H, CH_2), 0.88 (t, J = 6.79 Hz, 3H, 9′-CH_3). ^{13}C NMR (75 MHz, $CDCl_3$): δ 191.99 (CHO), 150.46 (C4), 134.33 (C1), 129.84 (C2, 6), 129.02 (C3, 5), 36.17 (C1′), 31.82 (C2′), 31.04, 29.45, 29.40, 29.25, 29.20, 22.62 (C8′), 14.06 (C9′). MS (FAB) *m/z* 233 (MH^+). HRMS (FAB) calcd for $C_{16}H_{25}O$ (MH^+), 233.1905; found, 233.1912.

(2*R*,4*R*)- and (2*S*,4*R*)-2-Decylthiazolidine-4-carboxylic Acid (1). Compound **1** was synthesized from L-cysteine hydrochloride monohydrate and 1-undecanal according to a procedure described previously.[37] Compound **1** was obtained as a colorless powder (1.01 g, 3.69 mmol, 69%); mp 154−155 °C (lit.[38] 153−154 °C). ^{1}H NMR (300 MHz, CD_3OD): δ 4.73 (dd, J = 8.89, 5.14 Hz, app 0.5H, 2-CH), 4.59 (dd, J = 8.07, 5.51 Hz, app 0.5H, 2-CH), 4.29 (t, J = 6.97 Hz, app 0.5H, 4-CH), 4.08 (t, J = 7.71 Hz, app 0.5H, 4-CH), 3.41−3.32 (m, app 1.5H, 5-CH_2), 3.15 (dd, J = 11.01, 8.26 Hz, app 0.5H, 5-CH_2), 2.06−2.01 (m, 1H, 1′-CH_2), 1.82−1.70 (m, 1H, 1′-CH_2), 1.45−1.29 (m, 16H, CH_2), 0.89 (t, J = 6.61 Hz, 3H, 10′-CH_3). ^{13}C NMR (75 MHz, DMSO-d_6): δ 172.87 (C=O), 172.32 (C=O), 71.07 (C4), 70.34 (C4), 65.21 (C2), 64.13 (C2), 36.98 (C1′), 36.71 (C1′), 34.82, 31.28, 28.96 (C5), 28.94 (C5), 28.88 (C2′), 28.83 (C2′), 28.77, 28.69, 27.57, 27.37, 22.09 (C9′), 13.94 (C10′). MS (ESI) *m/z* 274 (MH^+). Anal. ($C_{14}H_{27}NO_2S$) calcd: C, 61.50; H, 9.95; N, 5.12. Found: C, 61.33; H, 9.77; N, 5.09.

(2*R*,4*R*)- and (2*S*,4*R*)-2-Undecylthiazolidine-4-carboxylic Acid (2). Compound **2** was prepared according to the procedure described for **1** but using 1-dodecanal instead of 1-undecanal. Compound **2** was obtained as a colorless powder (941 mg, 3.27 mmol, 53%); mp 153−154 °C (lit.[38] 151−152 °C). ^{1}H NMR (300 MHz, CD_3OD): δ 4.75 (dd, J = 9.18, 5.14 Hz, app 0.5H, 2-CH), 4.59 (dd, J = 8.08, 5.51 Hz, app 0.5H, 2-CH), 4.30 (t, J = 6.98 Hz, app 0.5H, 4-CH), 4.09 (t, J = 7.34 Hz, app 0.5H, 4-CH), 3.42−3.27 (m, app 1.5H, 5-CH_2), 3.16 (dd, J = 11.19, 8.07 Hz, app 0.5H, 5-CH_2), 2.04−2.00 (m, 1H, 1′-CH_2), 1.84−1.76 (m, 1H, 1′-CH_2), 1.43−1.29 (m, 14H, CH_2), 0.89 (t, J = 6.97 Hz, 3H, 9′-CH_3). ^{13}C NMR (75 MHz, DMSO-d_6): δ

172.89 (C=O), 172.31 (C=O), 71.09 (C4), 70.38 (C4), 65.21 (C2), 64.13 (C2), 36.98 (C1′), 36.69 (C1′), 34.82, 31.29, 28.92 (C5), 28.89 (C5), 28.83 (C2′), 28.79 (C2′), 28.65, 27.57, 27.34, 22.09 (C10′), 13.95 (C11′). MS (ESI) *m/z* 288 (MH^+). Anal. ($C_{15}H_{29}NO_2S$) calcd: C, 62.67; H, 10.17; N, 4.87. Found: C, 62.57; H, 9.95; N, 5.05.

(2*R*,4*R*)- and (2*S*,4*R*)-2-Hexylthiazolidine-4-carboxylic Acid (3). Compound **3** was prepared according to the procedure described for **1** but using 1-heptanal instead of 1-undecanal. Compound **3** was obtained as a colorless powder (650 mg, 2.99 mmol, 49%); mp 149−150 °C. ^{1}H NMR (300 MHz, CD_3OD): δ 4.73 (dd, *J* = 9.18, 5.32 Hz, app 0.5H, 2-CH), 4.58 (dd, *J* = 8.08, 5.51 Hz, app 0.5H, 2-CH), 4.30 (t, *J* = 6.80 Hz, app 0.5H, 4-CH), 4.07 (t, *J* = 7.34 Hz, app 0.5H, 4-CH), 3.42−3.32 (m, app 1.5H, 5-CH_2), 3.15 (dd, *J* = 11.01, 8.17 Hz, app 0.5H, 5-CH_2), 2.04−1.99 (m, 1H, 1′-CH_2), 1.84−1.76 (m, 1H, 1′-CH_2), 1.38−1.33 (m, 8H, CH_2), 0.91 (t, *J* = 6.79 Hz, 3H, 7′-CH_3). ^{13}C NMR (75 MHz, DMSO-d_6): δ 172.86 (C=O), 172.33 (C=O), 71.08 (C4), 70.34 (C4), 65.27 (C2), 64.15 (C2), 36.99 (C1′), 36.65 (C1′), 34.83 (C4′), 31.16 (C3′), 28.47 (C5), 28.41 (C5), 27.52 (C2′), 27.32 (C2′), 21.98 (C5′), 13.90 (C6′). MS (ESI) *m/z* 218 (MH^+). Anal. ($C_{10}H_{19}NO_2S$) calcd: C, 55.26; H, 8.81; N, 6.44. Found: C, 55.15; H, 8.66; N, 6.59.

(2*R*,4*R*)- and (2*S*,4*R*)-2-Nonylthiazolidine-4-carboxylic Acid (4). Compound **4** was prepared according to the procedure described for **1** but using 1-decanal instead of 1-undecanal. Compound **4** was obtained as a colorless powder (1.09 g, 4.20 mmol, 69%); mp 153−154 °C (lit.[38] 156−157 °C). ^{1}H NMR (300 MHz, CD_3OD): δ 4.73 (dd, *J* = 8.99, 5.14 Hz, app 0.5H, 2-CH), 4.52 (dd, *J* = 8.26, 5.51 Hz, app 0.5H, 2-CH), 4.28 (t, *J* = 6.80 Hz, app 0.5H, 4-CH), 4.06 (t, *J* = 7.34 Hz, app 0.5H, 4-CH), 3.42−3.35 (m, app 1.5H, 5-CH_2), 3.13 (dd, *J* = 11.01, 7.07 Hz, app 0.5H, 5-CH_2), 2.06−1.99 (m, 1H, 1′-CH_2), 1.83−1.76 (m, 1H, 1′-CH_2), 1.35−1.29 (m, 14H, CH_2), 0.90 (t, *J* = 6.97 Hz, 3H, 9′-CH_3). ^{13}C NMR (75 MHz, DMSO-d_6): δ 172.85 (C=O), 172.33 (C=O), 71.05 (C4), 70.29 (C4), 65.29 (C2), 64.14 (C2), 37.01 (C1′), 36.75 (C1′), 34.82, 31.26, 28.93 (C5), 28.88 (C5), 28.82 (C2′), 28.75 (C2′), 28.65, 27.55, 27.34, 22.07 (C8′), 13.91 (C9′). MS (ESI) *m/z* 260 (MH^+). Anal. ($C_{13}H_{25}NO_2S$) calcd: C, 60.19; H, 9.71; N, 5.40. Found: C, 60.09; H, 9.54; N, 5.59.

(2*R*,4*R*)- and (2*S*,4*R*)-2-Dodecylthiazolidine-4-carboxylic Acid (5). Compound **5** was prepared according to the procedure described for **1** but using 1-tridecanal instead of 1-undecanal. Compound **5** was obtained as a colorless powder (1.32 g, 4.38 mmol, 71%); mp 151−152 °C. ^{1}H NMR (300 MHz, CD_3OD): δ 4.74 (dd, *J* = 8.99, 5.08 Hz, app 0.5H, 2-CH), 4.60 (dd, *J* = 8.26, 5.01 Hz, app 0.5H, 2-CH), 4.30 (t, *J* = 6.79 Hz, app 0.5H, 4-CH), 4.10 (t, *J* = 7.52 Hz, app 0.5H, 4-CH), 3.42−3.37 (m, app 1.5H, 5-CH_2), 3.17 (dd, *J* = 11.19, 8.08 Hz, app 0.5H, 5-CH_2), 2.07−2.00 (m, 1H, 1′-CH_2), 1.84−1.76 (m, 1H, 1′-CH_2), 1.32−1.30 (m, 20H, CH_2), 0.90 (t, *J* = 6.79 Hz, 3H, 12′-CH_3). ^{13}C NMR (75 MHz, DMSO-d_6): δ 172.85 (C=O), 172.28 (C=O), 71.07 (C4), 70.33 (C4), 65.16 (C2), 64.11 (C2), 36.95 (C1′), 36.68 (C1′), 34.81, 31.27, 28.98 (C5), 28.92 (C5), 28.86 (C2′), 28.80 (C2′), 28.75, 28.68, 27.55, 28.68, 27.55, 27.35, 22.07 (C11′), 13.91 (C12′). MS (ESI) *m/z* 302 (MH^+). Anal. ($C_{16}H_{31}NO_2S$) calcd: C, 63.74; H, 10.36; N, 4.65. Found: C, 63.68; H, 10.18; N, 4.83.

(2*R*,4*R*)- and (2*S*,4*R*)-2-Tridecylthiazolidine-4-carboxylic Acid (6). Compound **6** was prepared according to the procedure described for **1** but using 1-tetradecanal instead of 1-undecanal. Compound **6** was obtained as a colorless powder (1.41 g, 4.47 mmol, 73%); mp 151−152 °C (lit.[38] 148−149 °C). ^{1}H NMR (300 MHz, CD_3OD): δ 4.73 (dd, *J* = 8.99, 5.14 Hz, app 0.5H, 2-CH), 4.58 (dd, *J* = 8.26, 5.51 Hz, app 0.5H, 2-CH), 4.29 (t, *J* = 7.17 Hz, app 0.5H, 4-CH), 4.07 (t, *J* = 7.52 Hz, app 0.5H, 4-CH), 3.42−3.35 (m, app 1.5H, 5-CH_2), 3.14 (dd, *J* = 11.01, 8.07 Hz, app 0.5H, 5-CH_2), 2.04−2.01 (m, 1H, 1′-CH_2), 1.83−1.76 (m, 1H, 1′-CH_2), 1.35−1.29 (m, 22H, CH_2), 0.90 (t, *J* = 6.97 Hz, 3H, 13′-CH_3). ^{13}C NMR (75 MHz, DMSO-d_6): δ 172.87 (C=O), 172.32 (C=O), 71.10 (C4), 70.36 (C4), 65.23 (C2), 64.14 (C2), 36.98 (C1′), 36.68 (C1′), 34.82, 31.27, 28.99, 28.69, 27.55, 27.36, 22.07 (C12′), 13.93 (C13′). MS (ESI) *m/z* 316 (MH^+). Anal. ($C_{17}H_{33}NO_2S$) calcd: C, 64.71; H, 10.54; N, 4.44. Found: C, 64.69; H, 10.31; N, 4.64.

(2*R*,4*R*)- and (2*S*,4*R*)-2-Decylthiazolidine-4-carboxylic Acid (7). Compound **7** was prepared according to the procedure described for **1** but using D-cysteine instead of L-cysteine. Compound **7** was obtained as a colorless powder (1.01 g, 3.69 mmol, 60%); mp 153−154 °C. ^{1}H NMR (300 MHz, CD_3OD): δ 4.74 (dd, *J* = 8.81, 5.14 Hz, app 0.5H, 2-CH), 4.60 (dd, *J* = 8.26, 5.69 Hz, app 0.5H, 2-CH), 4.30 (t, *J* = 7.16 Hz, app 0.5H, 4-CH), 4.09 (t, *J* = 7.52 Hz, app 0.5H, 4-CH), 3.42−3.37 (m, app 1.5H, 5-CH_2), 3.16 (dd, *J* = 11.10, 8.26 Hz, app 0.5H, 5-CH_2), 2.06−2.00 (m, 1H, 1′-CH_2), 1.84−1.76 (m, 1H, 1′-CH_2), 1.31−1.27 (m, 16H, CH_2), 0.90 (t, *J* = 6.79 Hz, 3H, 10′-CH_3). ^{13}C NMR (75 MHz, DMSO-d_6): δ 172.84 (C=O), 172.28 (C=O), 71.06 (C4), 70.32 (C4), 65.16 (C2), 64.11 (C2), 36.95 (C1′), 36.68 (C1′), 34.81, 31.27, 28.96 (C5), 28.93 (C5), 28.87 (C2′), 28.81 (C2′), 28.76, 27.68, 27.55, 27.35, 22.07 (C9′), 13.91 (C10′). MS (ESI) *m/z* 274 (MH^+). Anal. ($C_{14}H_{27}NO_2S$) calcd: C, 61.50; H, 9.95; N, 5.12. Found: C, 61.42; H, 9.84; N, 5.30.

(2*R*,4*R*)- and (2*S*,4*R*)-2-(*m*-Pentylphenyl)thiazolidine-4-carboxylic Acid (19). Compound **19** was prepared according to the procedure described for **1** but using *m*-pentylbenzaldehyde **13** instead of 1-undecanal. Compound **19** was obtained as a colorless powder (206 mg, 0.74 mmol, 40%); mp 153−154 °C. ^{1}H NMR (300 MHz, CD_3OD): δ 7.38−7.28 (m, 4H, ArH), 5.73 (s, app 0.5H, 2-CH), 5.55 (s, app 0.5H, 2-CH), 4.40 (dd, *J* = 7.81, 4.34 Hz, app 0.5H, 4-CH), 4.08 (t, *J* = 7.52 Hz, app 0.5H, 4-CH), 3.51 (dd, *J* = 10.46, 7.52 Hz, app 1H, 5-CH_2), 3.39 (dd, *J* = 15.78, 4.93 Hz, app 1H, 5-CH_2), 2.63 (t, *J* = 7.34 Hz, 2H, 1′-CH_2), 1.66−1.63 (m, 2H, 2′-CH_2), 1.36−1.34 (m, 4H, CH_2), 0.88 (t, *J* = 7.16 Hz, 3H, 5′-CH_3). ^{13}C NMR (75 MHz, DMSO-d_6): δ 173.02 (C=O), 172.22 (C=O), 142.66 (ArC3), 142.36 (ArC3), 140.91 (ArC1), 138.77 (ArC1), 128.36 (ArC2), 128.25 (ArC5), 128.12 (ArC2) 127.57 (ArC5), 127.11 (ArC4), 126.83 (ArC4), 124.63 (ArC6), 124.33 (ArC6), 71.87 (C4), 71.24 (C4), 65.43 (C2), 64.88 (C2), 38.41 (C5′), 37.94 (C5′), 35.09 (C1′), 35.03 (C1′), 30.92 (C2′), 30.66 (C2′), 21.94 (C4′), 13.92 (C5′). MS (ESI) *m/z* 280 (MH^+). Anal. ($C_{15}H_{21}NO_2S$) calcd: C, 64.48; H, 7.58; N, 5.01. Found: C, 64.33; H, 7.58; N, 5.19.

(2*R*,4*R*)- and (2*S*,4*R*)-2-(*m*-Heptylphenyl)thiazolidine-4-carboxylic Acid (20). Compound **20** was prepared according to the procedure described for **1** but using *m*-heptylbenzaldehyde **14** instead of 1-undecanal. Compound **20** was obtained as a colorless powder (49 mg, 0.16 mmol, 50%); mp 142−144 °C. ^{1}H NMR (300 MHz, CD_3OD): δ 7.37−7.28 (m, 4H, ArH), 5.73 (s, app 0.5H, 2-CH), 5.55 (s, app 0.5H, 2-CH), 4.40 (dd, *J* = 7.16, 4.77 Hz, app 0.5H, 4-CH), 4.08 (t, *J* = 7.16 Hz, app 0.5H, 4-CH), 3.51 (dd, *J* = 10.64, 7.16 Hz, app 1H, 5-CH_2), 3.40 (dd, *J* = 11.01, 4.77 Hz, app 1H, 5-CH_2), 2.63 (t, *J* = 8.08 Hz, 2H, 1′-CH_2), 1.64−1.62 (m, 2H, 2′-CH_2), 1.33−1.30 (m, 8H, CH_2), 0.89 (t, *J* = 6.42 Hz, 3H, 7′-CH_3). ^{13}C NMR (75 MHz, DMSO-d_6): δ 173.27 (C=O), 172.45 (C=O), 142.92 (ArC3), 142.62 (ArC3), 141.17 (ArC1), 139.03 (ArC1), 128.62 (ArC2), 128.50 (ArC5), 128.38 (ArC2) 127.84 (ArC5), 127.37 (ArC4), 127.09 (ArC4), 124.89 (ArC6), 124.58 (ArC6), 72.13 (C4), 71.49 (C4), 65.68 (C2), 65.13 (C2), 38.67 (C5), 38.21 (C5), 35.38 (C1′), 35.32 (C1′), 31.51 (C2′), 31.25 (C2′), 28.91, 28.77, 22.33 (C6′), 14.21 (C7′). MS (ESI) *m/z* 308 (MH^+). Anal. ($C_{17}H_{25}NO_2S$) calcd: C, 66.41; H, 8.20; N, 4.56. Found: C, 66.33; H, 8.10; N, 4.74.

(2*R*,4*R*)- and (2*S*,4*R*)-2-(*m*-Nonylphenyl)thiazolidine-4-carboxylic Acid (21). Compound **21** was prepared according to the procedure described for **1** but using *m*-nonylbenzaldehyde **15** instead of 1-undecanal. Compound **21** was obtained as a colorless powder (356 mg, 1.06 mmol, 62%); mp 130−131 °C. ^{1}H NMR (300 MHz, CD_3OD): δ 7.37−7.16 (m, 4H, ArH), 5.73 (s, app 0.5H, 2-CH), 5.56 (s, app 0.5H, 2-CH), 4.42 (dd, *J* = 7.16, 4.77 Hz, app 0.5H, 4-CH), 4.10 (t, *J* = 7.52 Hz, app 0.5H, 4-CH), 3.50 (dd, *J* = 10.54, 7.52 Hz, app 1H, 5-CH_2), 3.40 (dd, *J* = 10.83, 4.77 Hz, app 1H, 5-CH_2), 2.63 (t, *J* = 7.89 Hz, 2H, 1′-CH_2), 1.63−1.60 (m, 2H, 2′-CH_2), 1.33−1.29 (m, 12H, CH_2), 0.89 (t, *J* = 6.97 Hz, 3H, 9′-CH_3). ^{13}C NMR (75 MHz, DMSO-d_6): δ 173.01 (C=O), 172.21 (C=O), 142.65

(ArC3), 142.35 (ArC3), 140.92 (ArC1), 138.75 (ArC1), 128.34 (ArC2), 128.24 (ArC5), 128.11 (ArC2) 127.56 (ArC5), 127.11 (ArC4), 126.84 (ArC4), 124.62 (ArC6), 124.31 (ArC6), 71.87 (C4), 71.24 (C4), 65.43 (C2), 64.88 (C2), 38.42 (C5), 37.95 (C5), 35.12 (C1′), 35.07 (C1′), 32.42, 31.27 (C2′), 30.98 (C2′), 28.98, 28.97, 28.86, 28.69, 22.09 (C8′), 13.95 (C9′). MS (ESI) *m/z* 336 (MH^+). Anal. ($C_{19}H_{29}NO_2S$) calcd: C, 68.02; H, 8.71; N, 4.17. Found: C, 67.80; H, 8.51; N, 4.40.

(2*R*,4*R*)- and (2*S*,4*R*)-2-(*p*-Pentylphenyl)thiazolidine-4-carboxylic Acid (22). Compound **22** was prepared according to the procedure described for **1** but using *p*-pentylbenzaldehyde **16** instead of 1-undecanal. Compound **22** was obtained as a colorless powder (182 mg, 0.65 mmol, 60%); mp 159−160 °C. ^{1}H NMR (300 MHz, CD_3OD): 7.46 (dd, J = 8.07, 3.30 Hz, 2H, ArH), 7.21 (dd, J = 3.30, 8.07 Hz, 2H, ArH), 5.73 (s, app 0.5H, 2-CH), 5.55 (s, app 0.5H, 2-CH), 4.40 (dd, J = 12.84, 4.96 Hz, app 0.5H, 4-CH), 4.07 (t, J = 7.34 Hz, app 0.5H, 4-CH), 3.54−3.48 (m, app 1H, 5-CH_2), 3.40 (dd, J = 11.02, 4.96 Hz, app 1H, 5-CH_2), 2.62 (t, J = 8.81 Hz, 2H, 1′-CH_2), 1.64−1.62 (m, 2H, 2′-CH_2), 1.34−1.31 (m, 4H, CH_2), 0.89 (t, J = 7.16 Hz, 3H, 5′-CH_3). ^{13}C NMR (75 MHz, DMSO-d_6): δ 173.02 (C=O), 172.24 (C=O), 142.54 (ArC4), 142.80 (ArC4), 138.24 (ArC1), 136.09 (ArC1), 128.36 (ArC2, 6), 128.11 (ArC2, 6), 127.18 (ArC3, 5) 126.91 (ArC3, 5), 71.71 (C4), 71.10 (C4), 65.36 (C2), 64.84 (C2), 38.45 (C5), 37.93 (C5), 34.77 (C1′), 34.74 (C1′), 30.86 (C3′), 30.62 (C2′), 30.59 (C2′), 21.94 (C4′), 13.91 (C5′). MS (ESI) *m/z* 280 (MH^+). Anal. ($C_{15}H_{21}NO_2S$) calcd: C, 64.48; H, 7.58; N, 5.01. Found: C, 64.27; H, 7.59; N, 5.21.

(2*R*,4*R*)- and (2*S*,4*R*)-2-(*p*-Heptylphenyl)thiazolidine-4-carboxylic Acid (23). Compound **23** was prepared according to the procedure described for **1** but using *p*-heptylbenzaldehyde **17** instead of 1-undecanal. Compound **23** was obtained as a colorless powder (158 mg, 0.51 mmol, 77%); mp 154−156 °C. ^{1}H NMR (300 MHz, CD_3OD): 7.47 (dd, J = 8.07, 3.30 Hz, 2H, ArH), 7.21 (dd, J = 3.30, 8.07 Hz, 2H, ArH), 5.73 (s, app 0.5H, 2-CH), 5.56 (s, app 0.5H, 2-CH), 4.40 (dd, J = 7.34, 4.77 Hz, app 0.5H, 4-CH), 4.09 (t, J = 7.34 Hz, app 0.5H, 4-CH), 3.55−3.50 (m, app 1H, 5-CH_2), 3.45 (dd, J = 16.88, 4.77 Hz, app 1H, 5-CH_2), 2.61 (t, J = 7.16 Hz, 2H, 1′-CH_2), 1.63−1.61 (m, 2H, 2′-CH_2), 1.32−1.29 (m, 8H, CH_2), 0.89 (t, J = 6.97 Hz, 3H, 7′-CH_3). ^{13}C NMR (75 MHz, DMSO-d_6): δ 172.92 (C=O), 172.15 (C=O), 142.45 (ArC4), 141.69 (ArC4), 138.15 (ArC1), 136.00 (ArC1), 128.26 (ArC2, 6), 128.01 (ArC2, 6), 127.08 (ArC3, 5) 126.81 (ArC3, 5), 71.62 (C4), 71.00 (C4), 65.27 (C2), 64.75 (C2), 38.36 (C5), 37.83 (C5), 34.71 (C1′), 34.68 (C1′), 31.15, 30.86 (C2′), 30.83 (C2′), 28.52, 28.42, 21.98 (C6′), 13.85 (C7′). MS (ESI) *m/z* 308 (MH^+). Anal. ($C_{17}H_{25}NO_2S$) calcd: C, 66.41; H, 8.20; N, 4.56. Found: C, 66.25; H, 8.16; N, 4.76.

(2*R*,4*R*)- and (2*S*,4*R*)-2-(*p*-Nonylphenyl)thiazolidine-4-carboxylic Acid (24). Compound **24** was prepared according to the procedure described for **1** but using *p*-nonylbenzaldehyde **18** instead of 1-undecanal. Compound **24** was obtained as a colorless powder (135 mg, 0.40 mmol, 45%); mp 130−131 °C. ^{1}H NMR (300 MHz, CD_3OD): 7.46 (dd, J = 8.02, 3.30 Hz, 2H, ArH), 7.20 (dd, J = 3.30, 8.02 Hz, 2H, ArH), 5.74 (s, app 0.5H, 2-CH), 5.57 (s, app 0.5H, 2-CH), 4.41 (dd, J = 7.34, 4.95 Hz, app 0.5H, 4-CH), 4.10 (t, J = 7.34 Hz, app 0.5H, 4-CH), 3.55−3.50 (m, app 1H, 5-CH_2), 3.45 (dd, J = 16.88, 4.95 Hz, app 1H, 5-CH_2), 2.62 (t, J = 6.61 Hz, 2H, 1′-CH_2), 1.63−1.61 (m, 2H, 2′-CH_2), 1.32−1.89 (m, 12H, CH_2), 0.89 (t, J = 6.42 Hz, 3H, 9′-CH_3). ^{13}C NMR (75 MHz, DMSO-d_6): δ 173.00 (C=O), 172.23 (C=O), 142.53 (ArC4), 141.77 (ArC4), 138.25 (ArC1), 136.08 (ArC1), 128.34 (ArC2, 6), 128.08 (ArC2, 6), 127.15 (ArC3, 5) 126.88 (ArC3, 5), 71.71 (C4), 71.07 (C4), 65.37 (C2), 64.83 (C2), 38.46 (C5), 37.91 (C5), 34.79 (C1′), 34.75 (C1′), 31.24, 30.92 (C2′), 30.89 (C2′), 28.93, 28.84, 28.66, 28.62, 22.06 (C8′), 13.93 (C9′). MS (ESI) *m/z* 336 (MH^+). Anal. ($C_{19}H_{29}NO_2S$) calcd: C, 68.02; H, 8.71; N, 4.17. Found: C, 67.87; H, 8.48; N, 4.39.

(2*R,4*R**)- and (2*S**,4*R**)-2-Nonyl-1,3-thiazinane-4-carboxylic Acid (8).** 1-Decanal (500 mg, 3.69 mmol) was added to a stirred DL-homocysteine (500 mg, 3.69 mmol) in aqueous ethanol (75%, 100 mL). The reaction was refluxed for 12 h. After it was cooled to room temperature, the precipitate was filtered and washed with water and diethyl ether to give a colorless powder. Recrystallization from boiling isopropyl alcohol gave compound **8** as a colorless powder (611 mg, 2.23 mmol, 60%); mp 140−141 °C. ^{1}H NMR (300 MHz, CD_3OD): 4.67 (dd, J = 8.81, 4.96 Hz, app 0.3H, 2-CH), 4.30 (dd, J = 10.09, 4.04 Hz, app 0.7H, 2-CH), 3.90 (t, J = 4.59 Hz, app 0.3H, 4-CH), 3.51 (dd, J = 12.66, 2.75 Hz, app 0.7H, 4-CH), 3.04 (app t, app 0.6H, 6-CH_2), 2.86−2.80 (m, app 1.4H, 6-CH_2), 2.75−2.63 (m, 2H, 5-CH_2), 1.97−1.74 (m, 2H, 1′-CH_2), 1.35−1.28 (m, 14H, CH_2), 0.89 (t, J = 6.97 Hz, 3H, 9′-CH_3). ^{13}C NMR (75 MHz, DMSO-d_6): δ 173.36 (C=O), 61.22 (C4), 58.96 (C2), 38.67 (C6), 35.88 (C5), 31.28 (C1′), 28.91, 28.72, 28.68, 28.52, 27.49, 25.30, 22.09 (C8′), 13.94 (C9′). MS (ESI) *m/z* 274 (MH^+). Anal. ($C_{14}H_{27}NO_2S$) calcd: C, 61.50; H, 9.95; N, 5.12. Found: C, 61.47; H, 9.97; N, 5.29.

(2*R,4*R**)- and (2*S**,4*R**)-2-Decyl-1,3-thiazinane-4-carboxylic Acid (9).** Compound **9** was prepared according to the procedure described for **8** but using 1-undecanal instead of 1-decanal. Compound **9** was obtained as a colorless powder (560 mg, 1.95 mmol, 53%); mp 148−149 °C. ^{1}H NMR (300 MHz, CD_3OD): 4.66 (dd, J = 13.76, 4.96 Hz, app 0.3H, 2-CH), 4.31 (dd, J = 9.91, 3.85 Hz, app 0.7H, 2-CH), 3.90 (t, J = 4.58 Hz, app 0.3H, 4-CH), 3.49 (dd, J = 12.66, 2.75 Hz, app 0.7H, 4-CH), 3.04 (app t, app 0.6H, 6-CH_2), 2.86−2.81 (m, app 1.4H, 6-CH_2), 2.73−2.58 (m, 2H, 5-CH_2), 1.93−1.74 (m, 2H, 1′-CH_2), 1.33−1.30 (m, 16H, CH_2), 0.90 (t, J = 6.79 Hz, 3H, 10′-CH_3). ^{13}C NMR (75 MHz, DMSO-d_6): δ 173.34 (C=O), 61.20 (C4), 58.96 (C2), 38.67 (C6), 35.87 (C5), 31.30 (C1′), 28.98, 28.90, 28.71, 28.52, 27.49, 25.31, 22.10 (C9′), 13.95 (C10′). MS (ESI) *m/z* 288 (MH^+). Anal. ($C_{15}H_{29}NO_2S$) calcd: C, 62.67; H, 10.17; N, 4.87. Found: C, 62.65; H, 9.97; N, 5.05.

(2*R,4*R**)- and (2*S**,4*R**)-2-Undecyl-1,3-thiazinane-4-carboxylic acid (10).** Compound **10** was prepared according to the procedure described for **8** but using 1-dodecanal instead of 1-decanal. Compound **10** was obtained as a colorless powder (792 mg, 2.63 mmol, 71%); mp 150−151 °C. ^{1}H NMR (300 MHz, CD_3OD): 4.68 (dd, J = 8.63, 4.95 Hz, app 0.3H, 2-CH), 4.31 (dd, J = 9.91, 4.04 Hz, app 0.7H, 2-CH), 3.90 (t, J = 4.77 Hz, app 0.3H, 4-CH), 3.49 (dd, J = 12.66, 2.75 Hz, app 0.7H, 4-CH), 3.04 (app t, app 0.6H, 6-CH_2), 2.86−2.81 (m, app 1.4H, 6-CH_2), 2.72−2.60 (m, 2H, 5-CH_2), 1.93−1.77 (m, 2H, 1′-CH_2), 1.33−1.29 (m, 18H, CH_2), 0.90 (t, J = 6.97 Hz, 3H, 11′-CH_3). ^{13}C NMR (75 MHz, DMSO-d_6): δ 173.34 (C=O), 61.20 (C4), 58.96 (C2), 38.67 (C6), 35.87 (C5), 31.30 (C1′), 29.01, 28.97, 28.91, 28.72, 28.52, 27.49, 25.31, 22.10 (C10′), 13.94 (C11′). MS (ESI) *m/z* 302 (MH^+). Anal. ($C_{16}H_{31}NO_2S$) calcd: C, 63.74; H, 10.36; N, 4.65. Found: C, 63.78; H, 10.15; N, 4.83.

(2*R,4*R**)- and (2*S**,4*R**)-2-Dodecyl-1,3-thiazinane-4-carboxylic Acid (11).** Compound **11** was prepared according to the procedure described for **8** but using 1-tridecanal instead of 1-decanal. Compound **11** was obtained as a colorless powder (831 mg, 2.63 mmol, 71%); mp 146−147 °C. ^{1}H NMR (300 MHz, CD_3OD): 4.67 (dd, J = 8.49, 5.51 Hz, app 0.3H, 2-CH), 4.31 (dd, J = 9.91, 4.04 Hz, app 0.7H, 2-CH), 3.90 (t, J = 4.77 Hz, app 0.3H, 4-CH), 3.50 (dd, J = 12.66, 2.75 Hz, app 0.7H, 4-CH), 3.04 (app t, app 0.6H, 6-CH_2), 2.86−2.81 (m, app 1.4H, 6-CH_2), 2.75−2.60 (m, 2H, 5-CH_2), 1.94−1.73 (m, 2H, 1′-CH_2), 1.35−1.29 (m, 16H, CH_2), 0.90 (t, J = 7.16 Hz, 3H, 10′-CH_3). ^{13}C NMR (75 MHz, DMSO-d_6): δ 173.37 (C=O), 61.23 (C4), 58.92 (C2), 38.67 (C6), 35.91 (C5), 31.27 (C1′), 28.99, 28.93, 28.88, 28.69, 28.50, 27.48, 25.29, 22.08 (C11′), 13.93 (C12′). MS (ESI) *m/z* 316 (MH^+). Anal. ($C_{17}H_{33}NO_2S$) calcd: C, 64.71; H, 10.54; N, 4.44. Found: C, 64.64; H, 10.36; N, 4.63.

(2*R,4*R**)- and (2*S**,4*R**)-2-Tridecyl-1,3-thiazinane-4-carboxylic Acid (12).** Compound **12** was prepared according to the procedure described for **8** but using 1-tetradecanal instead of 1-decanal. Compound **12** was obtained as a colorless powder (408 mg, 1.24 mmol, 56%); mp 136−137 °C. ^{1}H NMR (300 MHz, CD_3OD): 4.70−4.66 (m, app 0.3H, 2-CH), 4.32 (dd, J = 9.91, 4.04 Hz, app 0.7H, 2-CH), 3.90 (app t, app 0.3H, 4-CH), 3.47 (dd, J = 12.66, 2.94 Hz, app 0.7H, 4-CH), 3.04 (app t, app 0.6H, 6-CH_2), 2.86−2.81 (m, app 1.4H, 6-CH_2), 2.63−2.59 (m, 2H, 5-CH_2), 1.92−1.77 (m, 2H, 1′-CH_2), 1.35−1.26 (m, 22H, CH_2), 0.90 (t, J = 6.98 Hz, 3H, 13′-CH_3). ^{13}C

NMR (75 MHz, DMSO-d_6): δ 173.38 (C=O), 61.23 (C4), 58.93 (C2), 38.67 (C6), 35.91 (C5), 31.28 (C1′), 29.00, 28.94, 28.70, 28.51, 27.49, 25.30, 22.09 (C12′), 13.93 (C13′). MS (ESI) *m/z* 330 (MH^+). Anal. ($C_{18}H_{35}NO_2S$) calcd: C, 65.60; H, 10.71; N, 4.25. Found: C, 65.52; H, 10.50; N, 4.45.

Acknowledgment. This work was supported by the Japan Health Science Foundation and a Grant-in-Aid for Scientific Research on Priority Areas (A) "Exploitation of Multi-Element Cyclic Molecules" from the Ministry of Education, Culture, Sports, Science and Technology, Japan. We also thank Ms. R. Hara at the Analytical Research Center, Chiba University, for performing mass spectroscopy.

References

(1) Lee, M. J.; Van Brocklyn, J. R.; Thangada, S.; Liu, C. H.; Hand, A. R.; Menzeleev, R.; Spiegel, S.; Hla, T. Sphingosine-1-phosphate as a ligand for the G protein-coupled receptor EDG-1. *Science* **1998**, *279*, 1552−1555.

(2) Van Brocklyn, J. R.; Lee, M. J.; Menzeleev, R.; Olivera, A.; Edsall, L.; Cuvillier, O.; Thomas, D. M.; Coopman, P. J.; Thangada, S.; Liu, C. H.; Hla, T.; Spiegel, S. Dual actions of sphingosine-1-phosphate: extracellular through the Gi-coupled receptor Edg-1 and intracellular to regulate proliferation and survival. *J. Cell Biol.* **1998**, *142*, 229−240.

(3) Cuvillier, O.; Pirianov, G.; Kleuser, B.; Vanek, P. G.; Coso, O. A.; Gutkind, S.; Spiegel, S. Suppression of ceramide-mediated programmed cell death by sphingosine-1-phosphate. *Nature* **1996**, *381*, 800−803.

(4) Olivera, A.; Spiegel, S. Sphingosine-1-phosphate as second messenger in cell proliferation induced by PDGF and FCS mitogens. *Nature* **1993**, *365*, 557−560.

(5) Glickman, M.; Malek, R. L.; Kwitek-Black, A. E.; Jacob, H. J.; Lee, N. H. Molecular cloning, tissue-specific expression, and chromosomal localization of a novel nerve growth factor-regulated G-protein- coupled receptor, nrg-1. *Mol. Cell. Neurosci.* **1999**, *14*, 141−152.

(6) Bandoh, K.; Aoki, J.; Hosono, H.; Kobayashi, S.; Kobayashi, T.; Murakami-Murofushi, K.; Tsujimoto, M.; Arai, H.; Inoue, K. Molecular cloning and characterization of a novel human G-protein-coupled receptor, EDG7, for lysophosphatidic acid. *J. Biol. Chem.* **1999**, *274*, 27776−27785.

(7) Graler, M. H.; Bernhardt, G.; Lipp, M. EDG6, a novel G-protein-coupled receptor related to receptors for bioactive lysophospholipids, is specifically expressed in lymphoid tissue. *Genomics* **1998**, *53*, 164−169.

(8) Van Brocklyn, J. R.; Tu, Z.; Edsall, L. C.; Schmidt, R. R.; Spiegel, S. Sphingosine 1-phosphate-induced cell rounding and neurite retraction are mediated by the G protein-coupled receptor H218. *J. Biol. Chem.* **1999**, *274*, 4626−4632.

(9) An, S.; Bleu, T.; Hallmark, O. G.; Goetzl, E. J. Characterization of a novel subtype of human G protein-coupled receptor for lysophosphatidic acid. *J. Biol. Chem.* **1998**, *273*, 7906−7910.

(10) Okamoto, H.; Takuwa, N.; Yatomi, Y.; Gonda, K.; Shigematsu, H.; Takuwa, Y. EDG3 is a functional receptor specific for sphingosine 1-phosphate and sphingosylphosphorylcholine with signaling characteristics distinct from EDG1 and AGR16. *Biochem. Biophys. Res. Commun.* **1999**, *260*, 203−208.

(11) Hecht, J. H.; Weiner, J. A.; Post, S. R.; Chun, J. Ventricular zone gene-1 (vzg-1) encodes a lysophosphatidic acid receptor expressed in neurogenic regions of the developing cerebral cortex. *J. Cell Biol.* **1996**, *135*, 1071−1083.

(12) Racke, K.; Hammermann, R.; Juergens, U. R. Potential role of EDG receptors and lysophospholipids as their endogenous ligands in the respiratory tract. *Pulm. Pharmacol. Ther.* **2000**, *13*, 99−114.

(13) Pyne, S.; Pyne, N. Sphingosine 1-phosphate signaling via the endothelial differentiation gene family of G-protein-coupled receptors. *Pharmacol. Ther.* **2000**, *88*, 115−131.

(14) Pyne, S.; Pyne, N. J. Sphingosine 1-phosphate signaling in mammalian cells. *Biochem. J.* **2000**, *349*, 385−402.

(15) Sato, K.; Tomura, H.; Igarashi, Y.; Ui, M.; Okajima, F. Possible involvement of cell surface receptors in sphingosine 1-phosphate-induced activation of extracellular signal-regulated kinase in C6 glioma cells. *Mol. Pharmacol.* **1999**, *55*, 126−133.

(16) An, S.; Zheng, Y.; Bleu, T. Sphingosine 1-phosphate-induced cell proliferation, survival, and related signaling events mediated by G protein-coupled receptors Edg3 and Edg5. *J. Biol. Chem.* **2000**, *275*, 288−296.

(17) Pyne, S.; Chapman, J.; Steele, L.; Pyne, N. J. Sphingomyelin-derived lipids differentially regulate the extracellular signal-regulated kinase 2 (ERK-2) and c-Jun N-terminal kinase (JNK) signal cascades in airway smooth muscle. *Eur. J. Biochem.* **1996**, *237*, 819−826.

(18) Wu, J.; Spiegel, S.; Sturgill, T. W. Sphingosine 1-phosphate rapidly activates the mitogen-activated protein kinase pathway by a G protein-dependent mechanism. *J. Biol. Chem.* **1995**, *270*, 11484−11488.

(19) Ancellin, N.; Hla, T. Differential pharmacological properties and signal transduction of the sphingosine 1-phosphate receptors EDG-1, EDG-3, and EDG-5. *J. Biol. Chem.* **1999**, *274*, 18997−19002.

(20) Wang, F.; Nobes, C. D.; Hall, A.; Spiegel, S. Sphingosine 1-phosphate stimulates rho-mediated tyrosine phosphorylation of focal adhesion kinase and paxillin in Swiss 3T3 fibroblasts. *Biochem. J.* **1997**, *324*, 481−488.

(21) Zhou, D.; Luini, W.; Bernasconi, S.; Diomede, L.; Salmona, M.; Mantovani, A.; Sozzani, S. Phosphatidic acid and lysophosphatidic acid induce haptotactic migration of human monocytes. *J. Biol. Chem.* **1995**, *270*, 25549−25556.

(22) Filippi, S.; Amerini, S.; Maggi, M.; Natali, A.; Ledda, F. Studies on the mechanisms involved in the ATP-induced relaxation in human and rabbit corpus cavernosum. *J. Urol.* **1999**, *161*, 326−331.

(23) Vitolo, O. V.; Ciotti, M. T.; Galli, C.; Borsello, T.; Calissano, P. Adenosine and ADP prevent apoptosis in cultured rat cerebellar granule cells. *Brain Res.* **1998**, *809*, 297−301.

(24) Take, Y.; Inouye, Y.; Nakamura, S.; Allaudeen, H. S.; Kubo, A. Comparative studies of the inhibitory properties of antibiotics on human immunodeficiency virus and avian myeloblastosis virus reverse transcriptases and cellular DNA polymerases. *J. Antibiot. (Tokyo)* **1989**, *42*, 107−115.

(25) Hoffman, R.; Cameron, L. Characterization of a scintillation proximity assay to detect modulators of transforming growth factor alpha (TGF alpha) binding. *Anal. Biochem.* **1992**, *203*, 70−75.

(26) Huang, Y. Q.; Li, J. J.; Nicolaides, A.; Zhang, W. G.; Friedman-Kien, A. E. Increased expression of fibroblast growth factors (FGFs) and their receptor by protamine and suramin on Kaposi's sarcoma-derived cells. *Anticancer Res.* **1993**, *13*, 887−890.

(27) Rolland, A.; Prost, A.; Thylefors, B. Review, after 3 years of the treatment with suramine, of a village suffering from onchocerciasis under entomological protection. *Rev. Int. Trach. Pathol. Ocul. Trop. Subtrop.* **1980**, *57*, 99−106.

(28) Parrill, A. L.; Wang, D. A.; Bautista, D. L.; Van Brocklyn, J. R.; Lorincz, Z.; Fischer, D. J.; Baker, D. L.; Liliom, K.; Spiegel, S.; Tigyi, G. Identification of Edg1 receptor residues that recognize sphingosine 1-phosphate. *J. Biol. Chem.* **2000**, *275*, 39379−39384.

(29) Parrill, A. L.; Baker, D. L.; Wang, D. A.; Fischer, D. J.; Bautista, D. L.; Van Brocklyn, J.; Spiegel, S.; Tigyi, G. Structural features of EDG1 receptor−ligand complexes revealed by computational modeling and mutagenesis. *Ann. N. Y. Acad. Sci.* **2000**, *905*, 330−339.

(30) *Rational Drug Design Software Catalyst 4.6*; Accelrys, San Diego, CA (see http://www.accelrys.com/catalyst).

(31) Kaminski, J. J.; Rane, D. F.; Rothofsky, M. L. Database mining using pharmacophore models to discover novel structural prototypes. *Pharmacophore Perception, Development, and Use in Drug Design*; IUL Biotechnology Series: La Jolla, California, 2000; pp 251−268.

(32) We will report the preparation and utility of this cell system in detail elsewhere.

(33) Smellie, A.; Kahn, S. D.; Teig, S. L. Analysis of conformational coverage. 2. Applications of conformational models. *J. Chem. Inf. Comput. Sci.* **1995**, *35*, 295−304.

(34) Smellie, A.; Kahn, S. D.; Teig, S. L. Analysis of conformational coverage. 1. Validation and estimation of coverage. *J. Chem. Inf. Comput. Sci.* **1995**, *35*, 285−294.

(35) Smellie, A.; Teig, S. L.; Towbin, P. Poling: Promoting conformational variation. *J. Comput. Chem.* **1995**, *16*, 171−187.

(36) Tamama, K.; Kon, J.; Sato, K.; Tomura, H.; Kuwabara, A.; Kimura, T.; Kanda, T.; Ohta, H.; Ui, M.; Kobayashi, I.; Okajima, F. Extracellular mechanism through the Edg family of receptors might be responsible for sphingosine-1-phosphate-induced regulation of DNA synthesis and migration of rat aortic smooth-muscle cells. *Biochem. J.* **2001**, *353*, 139−146.

(37) *Available Chemical Directory (ACD) database*; MDL Information Systems, Inc.; 216 599 compounds.

(38) Schmolka, I. R.; Spoerri, P. E. Thiazolidine chemistry. II, The preparation of 2-substituted thiazolidine-4-carboxylic acids. *J. Org. Chem.* **1957**, *22*, 943−946.

(39) Chun, J.; He, L.; Byun, H.; Bittman, R. Synthesis of ceramide analogues having the C(4)−C(5) bond of the long-chain base as part of an aromatioc or heteroaromatic system. *J. Org. Chem.* **2000**, *65*, 7634−7640.

(40) Greene, J.; Kahn, S.; Savoj, H.; Sprague, P.; Teig, S. Chemical Function Queries for 3D Database Search. *J. Chem. Inf. Comput. Sci.* **1994**, *34*, 1297−1308.

JM020080C

Japanese Journal of Physiology, 52, 403–408, 2002

Inhomogeneous Vasodilatory Responses of Rat Tail Arteries to Heat Stress: Evaluation by Synchrotron Radiation Microangiography

Eriko KUWABARA, Fujiya FURUYAMA*, Kunihisa ITO, Etsuro TANAKA, Naoichiro HATTAN, Hisanori FUJIKURA, Koji KIMURA, Takako GOTO, Takashi HAYASHI, Hiroyuki TAIRA, Yoshiro SHINOZAKI, Keiji UMETANI†, Kazuyuki HYODO‡, Kenkichi TANIOKA§, Ryo MOCHIZUKI‖, Toshiaki KAWAI¶, Shirosaku KOIDE, and Hidezo MORI#

Departments of Surgery, Physiology, and Cardiology, and Center for Regenerative Medicine, Tokai University School of Medicine, Isehara, 259–1193 Japan;
* Department of Neurophysiology and Brain Sciences, Nagoya City University Graduate School of Medical Sciences, Nagoya, 467–8601 Japan;
† Japan Synchrotron Radiation Research Institute, Sayo-gun, Hyogo, 679–5198 Japan;
‡ High Energy Accelerator Research Organization, Tsukuba, 305–0801 Japan;
§ NHK Science and Technical Research Laboratories, Tokyo, 157–8510 Japan;
‖ NHK Engineering Services Inc., Tokyo, 150–0042 Japan;
¶ Hamamatsu Photonics K.K., Hamamatsu, 430–8587 Japan;
and Department of Cardiac Physiology, National Cardiovascular # Center Research Institute, Suita, 565–8565 Japan

Abstract: Tail blood flow is crucial for dissipating body heat in rats. Angiographies are convenient tools to evaluate tail circulation. However, conventional angiographies do not have sufficient sensitivity or spatial resolution for small vessels. Recently, we developed a novel microangiographic system using monochromatic synchrotron radiation and a high-definition video camera system. Here, we report an evaluation of rat tail circulation under heat stress using the synchrotron radiation microangiographic system. We performed an experiment using the microangiography of the caudal artery before and after heating up WKAH/HkmSlc rats to rectal temperature of 39°C. The images were digitized and temporal subtraction was performed, and the diameters of caudal arteries were evaluated. After heating, the medial caudal artery was markedly dilated (320±53 to 853±243 μm in diameter, $p<0.001$), while no significant change was observed in the lateral caudal arteries (139±42 to 167±73 μm) and segmental anastomosing vessels. The heat stress allowed for visualization of the superficial caudal arteries with a diameter of approximately 60 μm, not visible prior to heating. Thus, synchrotron radiation microangiography demonstrated that the rat tail possessed dual sets of arteries; one set was highly sensitive to heat-induced vasodilation (medial caudal artery and superficial caudal arteries) and the other set was less sensitive (lateral caudal arteries and segmental anastomosing vessels). [Japanese Journal of Physiology, 52, 403–408, 2002]

Key words: angiography, heat stress, peripheral circulation, vascular control, vasodilation.

Vasodilation in the superficial region of the body (i.e., skin) plays an important role in dissipating body heat in humans [1], as vasodilation in the tail does in rats [2, 3]. The rat tail has one large artery, the medial caudal artery, and many small arteries. The small arteries are distributed both in the superficial and deep regions in the tail.

In vivo analyses of regional blood flow and/or va-

Received on June 11, 2002; accepted on August 15, 2002
Correspondence should be addressed to: Hidezo Mori, Department of Cardiac Physiology, National Cardiovascular Center Research Institute, Suita, 565–8565 Japan. Tel: +81–6–6833–5012 ext 2530, Fax: +81–6–6835–5416, E-mail: hidemori@ri.ncvc.go.jp

soreactivity in the rat tail have been done using various techniques (e.g., plethysmography [4–6], thermo-monitoring [2], microsphere [7], laser Doppler [7], and X-ray angiography [8, 9]). Thermo-monitoring and laser Doppler methods reflect the blood flow only in superficial regions, and the microsphere method often fails to evaluate arteriovenous anastomoses. Angiography is able to evaluate even deep vessels consecutively. However, conventional X-ray angiography has neither the sensitivity needed to detect small amounts of iodine contrast material nor the spatial resolution to quantitate the diameters of the small vessels. For example, quantification of the diameters is impossible in vessels with a diameter of less than 300 μm [10]. Recently, we developed a novel microangiographic system with high contrast resolution and high spatial resolution using monochromatic synchrotron radiation as an X-ray source and a high-definition video camera system as a detector [11]. This system allowed depiction of small vessels in the leg (collateral arteries) [12], intestinal organs (vasa recta and their submucosal communications) [13], brain (small branches arising from the canine circle of Willis) [10], heart (penetrating transmural artery) [14], and cancer tissue (angiogenic vessels) [15], and depiction of small branches (down to the fifth order) of the pancreatic duct [13]. This system using analog images also demonstrated that the heat stress caused vasodilation in the medial caudal artery but not in the abdominal cutaneous artery in rats [9].

The purpose of this study was to evaluate vasodilatory responses to heat stress of rat tail arteries distinguishing between superficial and deep regions using an animated synchrotron radiation microangiographic system and digital image processing with higher time-, spatial-, and contrast-resolutions.

MATERIALS AND METHODS

Animals. Fourteen WKAH/HkmSlc rats (Japan SLC Inc., Hamamatsu, Japan) weighing 350 to 450 g were used. The animals were anesthetized with intravenous infusion of ketamine hydrochloride (1.0 mg/kg/min) via a catheter placed in the femoral vein after intraperitoneal injection of 125 mg/kg of the same drug. All procedures were conducted in accordance with the Guiding Principles for the Care and Use of Animals approved by the Council of the Physiological Society of Japan.

Angiography. The fundamental design of our synchrotron radiation angiographic system has already been reported (Fig. 1) [9–16]. Briefly, monochromatic synchrotron radiation with an energy level of 33.3 keV was obtained with a silicon crystal from beamlines NE5 and BL-14 in the High Energy Accelerator Research Organization, Tsukuba, Japan. The contrast images were formed on a fluorescent screen in which a 20×20 mm area was scanned at 15 or 30 frames/s by a high-definition video camera with 1125 TV lines [17, 18], and then stored as a digital image in a memory system (20×20 mm area, 1,024×1,024 pixels, 12-bit/pixel). Time-, spatial-, and contrast-resolutions of the present system have been improved in comparison with those of former resolutions [9]. The present system had a spatial resolution of 25 μm (20 line pairs/mm studied with a MTF chart) and a time resolution of 33 or 67 ms. To improve contrast resolution, a temporal subtracted image was created on a computer from the digital images obtained immediately before and during contrast material injection. As for contrast resolution using a vascular phantom (Type 76-700, Nuclear Associates, New York, USA), the minimum size (0.5 mm of diameter) vascular phantom with a minimum concentration (2.5 mg/ml of iodine) was visualized through an acrylic block with a 75 mm thickness. Vessel diameter was

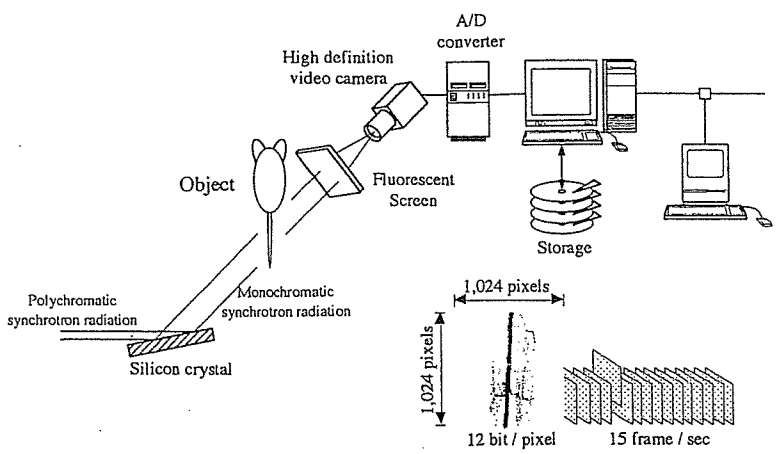

Fig. 1. Schematic presentation of the experimental setup. The contrast-enhanced images were formed on the fluorescent screen scanned by a high-definition video camera. Digital image processing was done on a computer.